

**Vortex structure in a d -wave superconductor
obtained by a confinement transition from the pseudogap metal**

Jia-Xin Zhang^{1,2} and Subir Sachdev²

¹*Institute for Advanced Study, Tsinghua University, Beijing 100084, China*

²*Department of Physics, Harvard University, Cambridge MA 02138, USA*

Abstract

We compute the structure of flux $h/(2e)$ vortices in a d -wave superconductor using a continuum SU(2) gauge theory of 2 flavors of charge e , SU(2)-fundamental Higgs bosons. Period-2 charge order is present near the vortex center. Upon coupling the electrons to the superconducting and charge order parameters, we find that the electronic local density of states does not have a zero-bias peak, in contrast to BCS theory. But there are sub-gap peaks at positive and negative bias, and these exhibit anti-phase periodic spatial modulations, as observed in scanning tunneling microscopy experiments in the underdoped cuprates (K. Matsuba *et al.*, J. Phys. Soc. Jpn. **76**, 063704 (2007)).

arXiv:2406.12964v1 [cond-mat.str-el] 18 Jun 2024

CONTENTS

I. Introduction	2
II. Continuum model for Higgs fields B_{\pm}	6
A. Flat configuration	8
B. Vison-like configuration	9
III. Electronic spectrum near the vortex	11
A. Effective electronic Hamiltonian	11
B. Vortex states of Dirac fermions	12
C. Induced local charging order near the vortex	15
IV. Discussion	19
Acknowledgements	21
A. Self-consistent calculation of B field	21
1. Flat configuration	21
2. Vison-like configuration	22
B. Derivation of LDOS Near the Vortex	23
References	28

I. INTRODUCTION

It is now well established that the superconducting state in the hole-doped cuprates has d -wave pairing [1]. Moreover, the 4 nodal fermionic quasiparticle excitations observed by photoemission [2] match the Bogoliubov quasiparticles expected after imposing d -wave pairing on a ‘large’ Fermi surface enclosing the Luttinger hole volume of $1 + p$, where p is hole-doping density away from the insulator. However, a closer look at the microstructure of the d -wave superconductor is provided by its Abrikosov vortex, and the pioneering scanning tunneling microscopy (STM) observations of Hoffman *et al.* [3] were not in agreement with the Bogoliubov-de Gennes theory of a d -wave superconductor with an underlying large Fermi surface. A complete understanding of their and subsequent observations [4–8], and their connection to the normal state electronic spectrum, remain key open problems in the physics of the cuprates.

Using the Bogoliubov-de Gennes theory, Wang and MacDonald [9] predicted a large zero-bias peak in the electronic local density of states (LDOS) at the core of each vortex. Such a peak has not been seen in numerous STM experiments [3–8], but has finally been observed [10] in heavily overdoped $\text{Bi}_2\text{Sr}_2\text{CaCu}_2\text{O}_{8+\delta}$; this observation is consistent with large Fermi surface present in the overdoped cuprates [2].

The focus of the present paper is on the underdoped cuprates, where the normal state above the superconducting critical temperature, T_c , is the ‘pseudogap metal’. This pseudogap metal does not have a large Fermi surface, and instead the photoemission spectrum is characterized by ‘Fermi arcs’ [2] (we will discuss a specific model for the pseudogap metal below). We will study the consequences of this electronic spectrum for the vortex below T_c . The STM investigations of the vortex structure [3–8] in the underdoped cuprates have revealed a number of remarkable features, not consistent the Bogoliubov-de Gennes theory of d -wave superconductivity in a large Fermi surface Fermi liquid:

- There is no Wang-MacDonald zero-bias peak.
- The zero-bias peak is replaced by sub-gap peaks at ± 6 -9 meV in the LDOS [4, 5].
- The LDOS at the sub-gap peaks exhibits periodic spatial modulations in a ‘halo’ around the vortex core. The modulations were initially observed to have a period of 4 lattice spacings [3–7], but a recent experiment [8] has seen an additional period 8 modulation. Period 8 modulations have also been observed in superconducting states without vortices [11–13], and have been interpreted by the co-existence of pair density waves and a uniform superconductor.
- There is an ‘anti-phase’ relation [5] between the LDOS modulations with positive and negative bias.

Many theories for the vortex structure in the underdoped regime [11, 14–23] commonly involve modeling with effective actions for multiple competing or intertwined orders, including antiferromagnetism, d -wave superconductivity, charge density wave, and pair density wave orders. Often implicit in these approaches is the assumption that the pseudogap state above T_c can be understood in terms of a theory of fluctuations of one or more of these orders [24–26].

We shall proceed here in the opposite direction, and regard the pseudogap metal as a quantum phase in its own right, and as the ‘parent’ of the ordered phases that emerge at low T . We model the pseudogap metal as a ‘fractionalized Fermi liquid’ (FL*) with hole pocket Fermi surfaces enclosing a volume p , along with a background spin liquid described by a $\text{SU}(2)$ gauge theory of fermionic spinons moving in a background π -flux [27]. Then the low temperature d -wave superconducting, antiferromagnetic, charge

density wave or pair density wave phases emerge upon a transition which confines the fractionalized excitations of the spin liquid.

The ancilla method [28] provides a powerful tool to describe the FL* pseudogap metal and its confinement transitions. Although it is possible to formulate our analysis without any reference to the ancilla method [29], we shall employ it as a convenient and foolproof method to connect to a lattice scale Hamiltonian, and to account for all anomalies in fractionalized phases. The ancilla method has been used in earlier work to describe

(i) the electronic photoemission spectrum of the FL* pseudogap metal, with the ‘Fermi arcs’ appearing as the front-sides of the hole pockets [30],

(ii) the onset of a uniform d -wave superconductor with 4 nodal quasiparticles from FL* [29, 31],

(iii) and the quantum oscillations in the charge-ordered state at low T and high fields [32].

Here, we shall use the ancilla method to describe the structure of the vortex that emerges upon the confinement transition from FL* to the d -wave superconductor.

The confinement is described by the condensation of a Higgs boson $B_{\mathbf{i}} \equiv (B_{1\mathbf{i}}, B_{2\mathbf{i}})$ which is a fundamental of the gauge SU(2), and carries charge e under the electromagnetic U(1); here \mathbf{i} denotes a square lattice site, and $B_{a\mathbf{i}}$ ($a = 1, 2$ is a SU(2) gauge index) are complex scalars. Then gauge-invariant bilinears of $B_{\mathbf{i}}$ determine the structure of the confining phase where $B_{\mathbf{i}}$ is condensed. The independent on-site and nearest-neighbor bilinears are [27]:

$$\begin{aligned}
\text{site charge density: } & \langle c_{\mathbf{i}\alpha}^\dagger c_{\mathbf{i}\alpha} \rangle \sim \rho_{\mathbf{i}} = B_{\mathbf{i}}^\dagger B_{\mathbf{i}} \\
\text{bond density: } & \langle c_{\mathbf{i}\alpha}^\dagger c_{\mathbf{j}\alpha} + c_{\mathbf{j}\alpha}^\dagger c_{\mathbf{i}\alpha} \rangle \sim Q_{\mathbf{ij}} = Q_{\mathbf{ji}} = \text{Im} \left(B_{\mathbf{i}}^\dagger e_{\mathbf{ij}} U_{\mathbf{ij}} B_{\mathbf{j}} \right) \\
\text{bond current: } & i \langle c_{\mathbf{i}\alpha}^\dagger c_{\mathbf{j}\alpha} - c_{\mathbf{j}\alpha}^\dagger c_{\mathbf{i}\alpha} \rangle \sim J_{\mathbf{ij}} = -J_{\mathbf{ji}} = \text{Re} \left(B_{\mathbf{i}}^\dagger e_{\mathbf{ij}} U_{\mathbf{ij}} B_{\mathbf{j}} \right) \\
\text{Pairing: } & \langle \varepsilon_{\alpha\beta} c_{\mathbf{i}\alpha} c_{\mathbf{j}\beta} \rangle \sim \Delta_{\mathbf{ij}} = \Delta_{\mathbf{ji}} = \varepsilon_{ab} B_{a\mathbf{i}} e_{\mathbf{ij}} U_{\mathbf{ij}} B_{b\mathbf{j}}.
\end{aligned} \tag{1.1}$$

Here \mathbf{i}, \mathbf{j} are nearest-neighbors on the square lattice, $U_{\mathbf{ij}}$ is the SU(2) lattice gauge field, ε is the unit antisymmetric tensor, and we have specified the interpretation of the bilinears in terms of the underlying electron operator $c_{\mathbf{i}\alpha}$ ($\alpha = \uparrow, \downarrow$ are SU(2) spin indices). The fixed field $e_{\mathbf{ij}} = -e_{\mathbf{ji}}$ specifies the π -flux of the spin liquid, and a choice is $e_{\mathbf{i}, \mathbf{i}+\hat{x}} = 1$, $e_{\mathbf{i}, \mathbf{i}+\hat{y}} = (-1)^x$.

A uniform d -wave superconductor has $\Delta_{\mathbf{i}, \mathbf{i}+\hat{x}} = -\Delta_{\mathbf{i}, \mathbf{i}+\hat{y}}$ but independent of \mathbf{i} , $\rho_{\mathbf{i}}$ and $Q_{\mathbf{ij}}$ spatially uniform, and $J_{\mathbf{ij}} = 0$. ‘Charge order’ can appear from spatial modulations in $\rho_{\mathbf{i}}$, $Q_{\mathbf{ij}}$, or $\Delta_{\mathbf{ij}}$, and modulations in $\Delta_{\mathbf{ij}}$ can be identified as pair density waves. But note that the configurations of these order parameters are all tied to the $B_{\mathbf{i}}$. Thus we can regard $B_{\mathbf{i}}$ as simultaneously a ‘square root’ of d -wave superconductivity, charge density wave, and pair density wave orders, and the different orientations of $B_{\mathbf{i}}$

describes the intertwining of these orders.

Ref. [27] presented an effective lattice action for the B_i and U_{ij} , along with its couplings to the fermionic spinons and the electronic quasiparticles. It would be of interest to study vortex lattice saddle points of this action in the presence of an applied magnetic field (similar to analyses in Ref. [23] for the Bogoliubov-de Gennes theory augmented by competing orders). However such a complete analysis would be numerically very demanding, and here we will limit ourselves to a simplified continuum limit for which analytic results are possible [27, 33]. The condensation of B_i in this limit can lead to charge order only with period of two lattice spacings. Longer period charge orders are possible in the theory of Ref. [27] (see also Ref. [32]), and we expect the main features of our results will generalize to more realistic situations. In this context, it is worth noting that for charge order periods longer than 2, the condensation of the B_i is at wavevectors $\pm \mathbf{Q}_{\text{cdw}}/2$, where \mathbf{Q}_{cdw} is the charge-ordering wavevector. In the presence of co-existing superconductivity, the orientation of B_i can also induce ‘pair density wave’ order at $\mathbf{Q}_{\text{cdw}}/2$, and we propose this as an origin of the observed period 8 modulations [8, 11–13].

We also note the relationship between our model for underdoped vortex structure and the analysis of Nagaosa, Lee, and Wen [34] (see also Refs. [35–40]). These authors also considered the condensation of complex scalars with quantum numbers similar to B_i , but in the context of a different ‘staggered flux’ spin liquid with a U(1) gauge field (which is unstable to a trivial U(1)-monopole [41, 42]). In their case, the condensation of B_i leads to d -wave superconductivity or current order, but no charge order.

Our continuum model for the B_i is described in Section II. It is expressed in terms of 2 SU(2) fundamental complex fields B_{as} , where $s = \pm$ is a ‘valley’ index, and a is the previously specified SU(2) gauge index. For bosons, valleys are determined by the minimum of the dispersion, and for the gauge choice of e_{ij} above, the valleys are chosen at wavevectors $\mathbf{Q}_+ = \frac{\pi}{2}(1, 1)$ and $\mathbf{Q}_- = \frac{\pi}{2}(1, -1)$. We obtain analytic results for the vortex with flux $h/(2e)$ in the continuum theory and show that the vicinity of the vortex core has charge order (for suitable choices of the quartic self-interactions of the B_{as}). There are some similarities to this vortex-induced charge order to earlier analyses [38–40] which used a dual model for the quantum fluctuations of the vortices.

Section III turns to a computation of the electronic spectrum in the background of the vortex obtained in Section II. We use a simplified continuum model in which the wavevector of the period-2 charge order is exactly equal to the separation between the nodal points of the superconductor. We find that the charge order has significant effects on the LDOS, and compare our results to STM data.

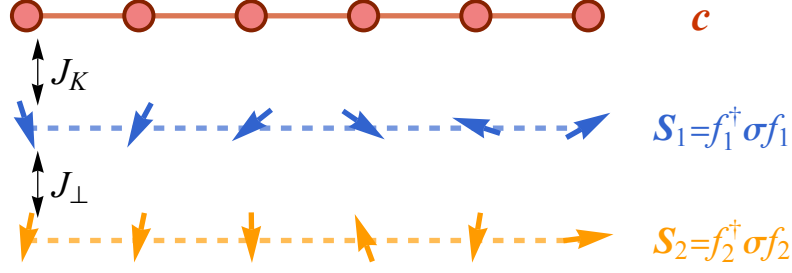


FIG. 1: Schematic illustration of the ancilla model. Red circles denote the actual electrons, while blue arrows in the second layer and orange arrows in the third layer represent ancilla spins \mathbf{S}_1 and \mathbf{S}_2 , respectively, which can be further fractionalized into spinons f_1 and f_2 . Black arrows between distinct layers indicate Kondo coupling J_K and rung-exchange J_\perp , respectively.

II. CONTINUUM MODEL FOR HIGGS FIELDS B_\pm

Here, we utilize the ancilla approach introduced in Ref. [27] to describe a single-band Hubbard model of electrons c with on-site repulsion U . This on-site repulsion U can be captured by coupling the c electrons to an insulated bilayer square lattice antiferromagnet composed of spin-1/2 moments \mathbf{S}_1 and \mathbf{S}_2 , as shown in Fig. 1. When the rung-exchange J_\perp in the bilayer antiferromagnet is much larger than the Kondo interaction J_K between the c electrons and \mathbf{S}_1 , the \mathbf{S}_1 and \mathbf{S}_2 spins form a trivial rung-singlet state. In this scenario, the c electrons are largely decoupled from the ancilla spins and form a large Fermi surface with Luttinger volume $1+p$, corresponding to the Fermi liquid phase in the overdoped regime. Conversely, when $J_\perp \ll J_K$, the ancilla spins \mathbf{S}_1 are expected to be Kondo screened by the c electrons, forming a Fermi pocket with a non-Luttinger volume p . Meanwhile, the \mathbf{S}_2 spins form a π -flux spin liquid. This latter case corresponds to the FL* phase, which is the focus of this work.

The corresponding Hamiltonian of the ancilla model is given by:

$$\begin{aligned}
 H = & \sum_{i,j} \left[t_{ij}^c c_i^\dagger c_j + t_{ij}^f f_{1,i,\sigma}^\dagger f_{1,j,\sigma} \right] + iJ \sum_{\langle i,j \rangle} f_{2,i,\sigma}^\dagger e_{ij} f_{2,j,\sigma} \\
 & + \sum_i \left[\Phi c_{i,\sigma}^\dagger f_{1,i,\sigma} + iB_1 f_{2,i,\sigma}^\dagger f_{1,i,\sigma} - iB_2 i\epsilon_{\alpha\beta} f_{2,i,\alpha} f_{1,i,\beta} + \text{H.c.} \right],
 \end{aligned} \tag{2.1}$$

where f_1 and f_2 are the fermionic partons of the ancilla spins $\mathbf{S}_1 = f_1^\dagger \boldsymbol{\sigma} f_1$ and $\mathbf{S}_2 = f_2^\dagger \boldsymbol{\sigma} f_2$ (with $\boldsymbol{\sigma}$ as the Pauli matrix), respectively. Here, t_{ij}^c and t_{ij}^f represent the hopping terms for physical c electrons and f_1 , while e_{ij} denotes the π -flux hopping for f_2 . Importantly, the hybridization field Φ and the chargin field B with a unit electromagnetic charge are introduced to decouple the Kondo interaction J_K and the rung-exchange J_\perp , respectively. The different phases of H are:

- The FL* pseudogap metal phase is obtained when $\Phi \neq 0$ and $B = 0$: then the c and f_1 fermions

hybridize to form the small hole pockets of size p , while the f_2 fermions realize the ‘spectator’ π -flux spin liquid.

- The Higgs/confinement transition to the superconductor is described by the condensation of the Higgs field B in a background with $\Phi \neq 0$. We study here the nature of this condensation in the presence of a $h/(2e)$ vortex in the superconducting phase. The choice between the order parameters in Eq. (1.1) is made by the orientation of the complex doublet (B_{1i}, B_{2i}) .
- The large Fermi surface Fermi liquid phase (FL) is obtained when $\Phi = 0$ and $B = 0$, and the $f_{1,2}$ fermions confine to form a rung-singlet phase. We do not study this FL phase or the FL-FL* transition [28, 43] in the present paper.

Following the analysis in Refs. [27, 33], the low-lying modes of the B field at the continuum limit can be regarded as a 4-component bosonic field. Two of these components are the gauge $SU(2)$ components, as shown in Eq. (2.1), while the other two correspond to two degenerate dispersion minima (two distinct valleys). Hence, the effective free energy of the chargin B in the continuum limit can be obtained by integrating out all the other fields in Eq. (2.1), resulting in:

$$F = \int d^2\mathbf{r} |(\nabla + i\mathbf{A}^e + i\mathbf{a}^z\sigma_z) B_s|^2 + mB_s^\dagger B_s + u \left(B_s^\dagger B_s \right)^2 \quad (2.2)$$

$$+ v_1 \left(\rho_{(\pi,0)}^2 + \rho_{(0,\pi)}^2 \right) + v_2 D^2 + v_3 |\Delta|^2 + \frac{1}{g} (\nabla \times \mathbf{A}^e)^2 + \frac{1}{\lambda} (\nabla \times \mathbf{a}^z)^2, ,$$

where the relevant conventional order parameters, consisting of bilinear terms of the B fields, are defined as:

$$\begin{aligned} d\text{-wave SC} : \quad \Delta &= \epsilon_{ab} B_{a+} B_{b-} \\ x\text{-CDW} : \quad \rho_{(\pi,0)} &= B_{a+}^\dagger B_{a+} - B_{a-}^\dagger B_{a-} \\ y\text{-CDW} : \quad \rho_{(0,\pi)} &= B_{a+}^\dagger B_{a-} + B_{a-}^\dagger B_{a+} \\ d\text{-density wave} : \quad D &= i \left(B_{a+}^\dagger B_{a-} - B_{a-}^\dagger B_{a+} \right). \end{aligned} \quad (2.3)$$

Here, Δ represents the d -wave superconducting (SC) order, $\rho_{(\pi,0)}$ and $\rho_{(0,\pi)}$ represent the period-2 charge density wave (CDW) along the x and y directions, respectively, while D represents the d -density wave order, which breaks time-reversal symmetry and is characterized by a circulating current pattern. In these equations, $s = \pm$ and $a = 1, 2$ represent the valley index and the gauge $SU(2)$ index of the B field, respectively. It is important to note that the CDW states above are primarily in the bond densities, Q_{ij} , in Eq. (1.1) [27, 33]; so when co-existing with superconductivity this will lead to pair density wave order represented by modulations in Δ_{ij} .

	B_{1+}	B_{2+}	B_{1-}	B_{2-}
\mathbf{A}^e	2π	2π	2π	2π
total	2π	2π	2π	2π

TABLE I: With the flat configuration of \mathbf{a}^z , the \mathbf{A}^e -flux and total flux experienced by B fields far from the vortex core.

As the mass m becomes negative, confinement occurs via the condensation of the chargin field B , leading to distinct possible conventional orders as defined in Eq. (2.3). The specific phase of the system is determined by the parameters v_1 , v_2 , and v_3 in Eq. (2.2). For our subsequent discussions, we choose these parameters so that the bulk system is in the d -wave superconducting phase. We hypothesize a solution by adopting an ansatz for B_{\pm} in the SC phase:

$$B_+ = b \begin{pmatrix} \cos \theta \\ \sin \theta \end{pmatrix}, \quad B_- = b \begin{pmatrix} -\sin \theta \\ \cos \theta \end{pmatrix} \quad (2.4)$$

where b and $\theta \in [0, 2\pi)$ are both real numbers. This leads to $\Delta = \epsilon_{ab} B_{a+} B_{b-} = b^2$ and $\rho_{(\pi,0)} = \rho_{(0,\pi)} = D = 0$, indicating a homogeneous superconducting phase without any coexisting order.

Next, we will explore the superconducting vortex states in the presence of an external magnetic field \mathbf{A}^e , and we will show that the vortex physics is intimately related to the internal gauge field \mathbf{a}^z , with coupling constants introduced by λ in Eq. (2.2). It is critical to note that while, in principle, bosonic chargons B_{\pm} carry fundamental SU(2) gauge charges (i.e., $i\mathbf{a}^j \sigma_j$), only the z -component is considered in Eq. (2.2) for simplicity. This simplification is justified by the fact that the three components of gauge fluctuation are completely frozen as the Higgs field B_{\pm} condenses in the superconducting phases.

A. Flat configuration

As $\lambda \rightarrow 0$, the cost of finite \mathbf{a}^z flux tends to infinity, so the flat gauge structure predominates, signifying $\mathbf{a}^z = 0$. In this scenario, the components of B_{\pm} can perceive the flux of \mathbf{A}^e , as summarized in Table I. Consequently, compared with Eq. (2.4), the ansatz for the chargin B is modified to:

$$B_+ = b \begin{pmatrix} \cos \theta \\ \sin \theta \end{pmatrix} f(r) e^{i\phi}, \quad B_- = b \begin{pmatrix} -\sin \theta \\ \cos \theta \end{pmatrix} f(r) e^{i\phi} \quad (2.5)$$

where $f(r) \in [0, 1]$ represents the amplitude modulation along the radial direction, and ϕ is the coordinate angle in the two-dimensional real space, encircling the pole $r = 0$ with 2π winding. Note that, in general, phase winding can be any integer multiple of 2π to satisfy the single-valued condition for the charge e

boson B_{\pm} . However, we only consider the lowest energy vortex in this context, corresponding to a 2π phase winding. Here, b and θ , which are inherited from Eq. (2.4), are independent of spatial coordinates.

Then, as shown in Fig. 2(a), one can determine the spatial dependence of $f(r)$ and $\Phi_A(r)$ by optimizing the free energy Eq. (2.2) after replacing the B field with the ansatz Eq. (2.5); see Appendix A 1. These results reveal that $f(r)$ is suppressed near the vortex core to prevent the divergence of kinetic energy. Additionally, the electromagnetic flux $\Phi_A(r) = \oint A^e(r) \cdot d\mathbf{l}$ asymptotically approaches 2π ($= hc/e \equiv 2\phi_0$ if the full units are restored) at distances far from the vortex core. Therefore, the order parameters, as defined in Eq. (2.3), are represented by:

$$\begin{aligned}
d\text{-wave SC} : \quad \Delta &= b^2 f^2(r) e^{i2\phi} \\
x\text{-CDW} : \quad \rho_{(\pi,0)} &= 0 \\
y\text{-CDW} : \quad \rho_{(0,\pi)} &= 0 \\
d\text{-density wave} : \quad D &= 0,
\end{aligned} \tag{2.6}$$

This configuration implies the formation of a 4π superconducting vortex, attributable to the phase 2ϕ , while all the other intertwined orders completely vanish. The spatial variation of the magnitudes of these order parameters is presented in Fig. 2(b), indicating that the superconducting order parameters diminish in proximity to the vortex core. Consequently, the trivial flat SU(2) gauge structure is capable of yielding 4π superconducting vortices exclusively, without the coexistence of any other order.

B. Vison-like configuration

On the other hand, as λ becomes large, contrary to the flat configuration, the existence of a vison-like configuration is allowed, characterized by a π flux structure in the gauge field \mathbf{a}^z :

$$\Phi_a(r) = \oint \mathbf{a}^z(r) \cdot d\mathbf{l} \xrightarrow{r \rightarrow \infty} \pi. \tag{2.7}$$

Due to the first term in Eq. (2.2), B_{as} with the opposite index of a perceive opposite fluxes of \mathbf{a}^z . Thus, the resulting total gauge structure perceived by B_{as} is summarized in Table II, suggesting that B_{1s} experiences a total 2π flux, leading to the 2π phase winding, while B_{2s} does not need to have any phase winding. In this context, the single-valued condition can still be well satisfied. Similarly, the B_{as} can be expressed as:

$$B_{\pm} = b \begin{pmatrix} \cos \theta f(r) e^{i\phi} \\ \sin \theta h(r) \end{pmatrix}, \quad B_{-} = b \begin{pmatrix} -\sin \theta f(r) e^{i\phi} \\ \cos \theta h(r) \end{pmatrix}. \tag{2.8}$$

Based on the ansatz of Eq. (2.8), the results of the spatial dependence for $\Phi_a(r)$, $\Phi_A(r)$, $f(r)$, and $h(r)$ are depicted in Fig. 2(c), illustrating that $f(r)$ is suppressed near the vortex core, while $h(r)$ remains

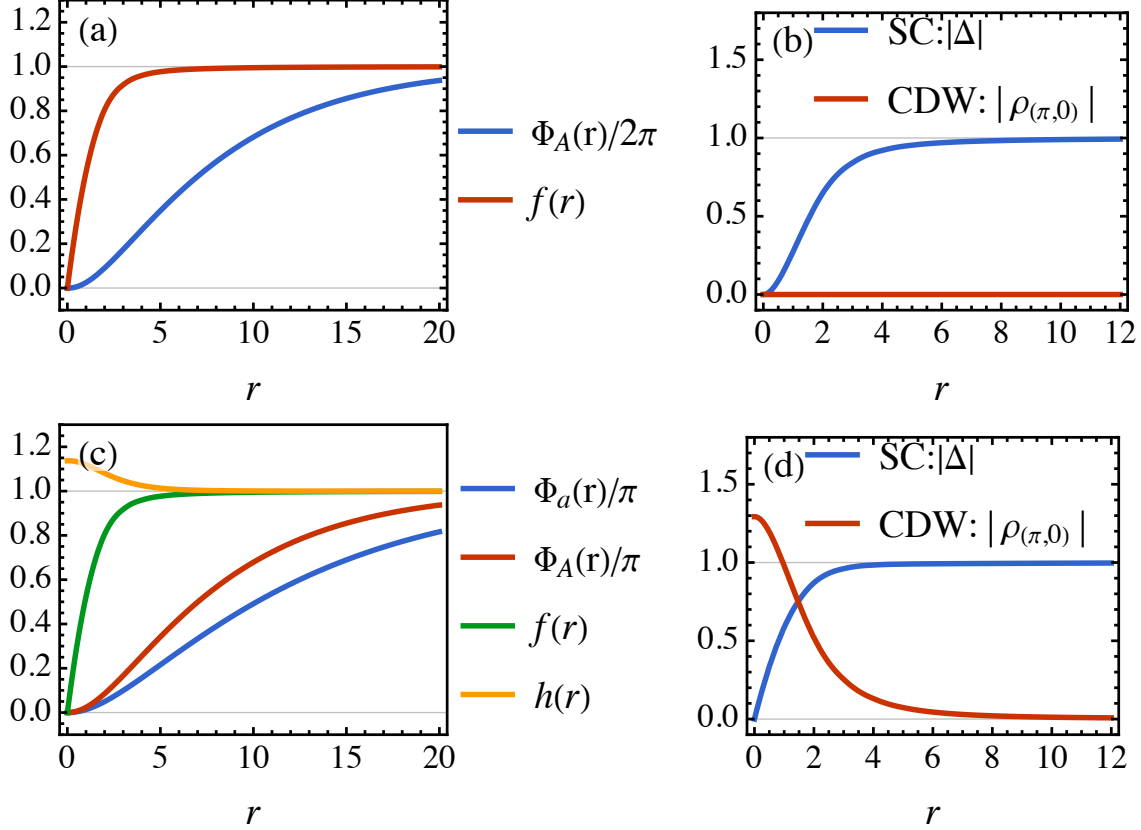


FIG. 2: (a)-(b) With the parameters: $m = -1$, $u = 2$, $v_3 = -1$, $g = 10u$. Spatial dependence of $\Phi_A(r)$ and $f(r)$ with the chargon B ansatz in Eq. (2.5) is shown in (a), and the corresponding magnitude of order parameter Δ and $\rho_{(\pi,0)}$ in Eq. (2.6) in (b). (c)-(d) With the parameters: $m = -1$, $u = 2$, $v_1 = 0.5$, $v_3 = -1$, $g = 10u$, $\lambda = g/9$. Spatial dependence of $\Phi_a(r)$, $\Phi_A(r)$, $f(r)$, and $h(r)$ with the chargon B ansatz in Eq. (2.8) is shown in (c), and the corresponding magnitude of order parameter Δ and $\rho_{(\pi,0)}$ in Eq. (2.9) in (d).

approximately constant; see Appendix A 2. The fluxes of both Φ_A and Φ_a converge to π ($= hc/2e \equiv \phi_0$ if the full units are restored) at distances far from the vortex core, satisfying the minimal flux quantization condition in superconductors. Then, the order parameters defined in Eq. (2.3) can be expressed as:

$$\begin{aligned}
 d\text{-wave SC} : \quad \Delta &= b^2 f(r) h(r) e^{i\phi} \\
 x\text{-CDW} : \quad \rho_{(\pi,0)} &= (f^2(r) - h^2(r)) b^2 \cos 2\theta \\
 y\text{-CDW} : \quad \rho_{(0,\pi)} &= (f^2(r) - h^2(r)) b^2 \sin 2\theta \\
 d\text{-density wave} : \quad D &= 0,
 \end{aligned} \tag{2.9}$$

This configuration implies the formation of a 2π superconducting vortex and the potential emergence of stripe-like CDW. The spatial variation in the magnitudes of these order parameters is shown in Fig. 2(d), indicating that the superconducting order parameters are suppressed near the vortex core, while CDW

	B_{1+}	B_{2+}	B_{1-}	B_{2-}
\mathbf{A}^e	π	π	π	π
\mathbf{a}^z	π	$-\pi$	π	$-\pi$
total	2π	0	2π	0

TABLE II: With the vison-like configuration of \mathbf{a}^z , the \mathbf{A}^e -flux, \mathbf{a}^z -flux, and total flux perceived by B fields far from the vortex core.

$\rho_{(\pi,0)}$ and $\rho_{(0,\pi)}$ become prominent within the vortex core.

As a result, in scenarios where λ is not negligible, the existence of a vison-like structure in the gauge field \mathbf{a}^z facilitates the formation of a 2π superconducting vortex, in which the core induces a local charge density wave. Notice that a excitation carrying π flux ‘trapped’ in the vortex is also necessary under the framework of other parton constructions[44–46] to obtain the correct flux quantization condition.

III. ELECTRONIC SPECTRUM NEAR THE VORTEX

A. Effective electronic Hamiltonian

This section will further study the single-particle spectrum near the vortex based on the configuration of the B field obtained in the last section at the continuum limit. The behavior of physical electrons in Eq. (2.1) can be described effectively after integrating out ancilla spinons f_1 and f_2 . Consequently, the resulting electronic Hamiltonian is given by:

$$H_c \equiv \sum_{\mathbf{k}} H_0 c_{\mathbf{k},\sigma}^\dagger c_{\mathbf{k},\sigma} + \frac{\Phi^2}{\gamma^2 J} \sum_{\langle i,j \rangle} \left((J_{ij} + iQ_{ij}) c_{i\sigma}^\dagger c_{j\sigma} + \Delta_{ij} \epsilon_{\alpha\beta} c_{i\alpha} c_{j\beta} \right) + \text{H.c.}, \quad (3.1)$$

where $\gamma = -(\epsilon_{\mathbf{k}=0}^{f_1})^{-1}$ and H_0 is frequency-dependent with the expression as:

$$H_0(\mathbf{k}, \omega) = \epsilon_{\mathbf{k}}^c + \frac{\Phi^2}{\omega - \epsilon_{\mathbf{k}}^{f_1}}, \quad (3.2)$$

where $\epsilon_{\mathbf{k}}^c$ and $\epsilon_{\mathbf{k}}^{f_1}$ are the bare dispersions for electrons c and spinons f_1 , respectively. These dispersions include the nearest neighbor terms (t^c , t^f), next nearest neighbor terms ($(t^c)'$, $(t^f)'$), next-next nearest neighbor terms ($(t^c)''$, $(t^f)''$), and next-next-next nearest neighbor terms ($(t^c)'''$) to fit the photo-emission data. Therefore, the corresponding spectral function

$$A_c(\mathbf{k}, \omega) = -\frac{1}{\pi} \text{Im} \frac{1}{\omega + i0^+ - H_0(\mathbf{k}, \omega + i0^+)}, \quad (3.3)$$

is shown in Fig. 3 (a) at $\omega = 0$, demonstrating Fermi arc behaviors. Moreover, the interaction couplings Δ_{ij} , J_{ij} , and Q_{ij} in Eq. (3.1) are combinations of the B field on the lattice [as defined in Eq. (1.1)], and

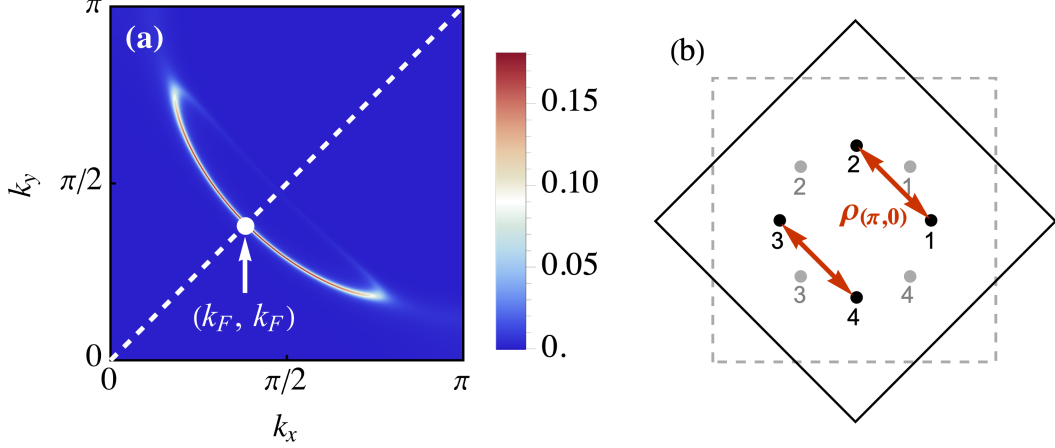


FIG. 3: With parameters $t^c = 200$, $(t^c)' = -34$, $(t^c)'' = -36$, $(t^c)''' = -7$, $t^f = -100$, $(t^f)' = 30$, $(t^f)'' = 10$, and doping density $\delta = 0.2$. (a) Spectral function of Eq. (3.3) at zero frequency. (b) Labeling of the four Dirac points, shown in gray before and in black after rotation, as described in Eq. (3.6). Red arrows indicate the x-CDW coupling $\rho(\pi, 0)$ connecting different Dirac points.

their relation with continuum order parameters in Eq. (2.3) are given by:

$$\begin{aligned}
 \Delta_{ij} &= \eta_{ij} 2(1 + \sqrt{2})\Delta \\
 J_{ij} &= -(1 + \sqrt{2})\rho_{(0,0)} + (-1)^{i_y}(2 + \sqrt{2})\rho_{(0,\pi)} \frac{1 - \eta_{ij}}{2} + (-1)^{i_x}(2 + \sqrt{2})\rho_{(\pi,0)} \frac{1 + \eta_{ij}}{2} \\
 Q_{ij} &= -(-1)^{i_x+i_y}(1 + \sqrt{2})D\eta_{ij}
 \end{aligned} \tag{3.4}$$

where $\eta_{i,i\pm\hat{x}} = -1$ and $\eta_{i,i\pm\hat{y}} = 1$. According to Eq. (3.4), it is explicitly shown that Δ_{ij} represents the d -wave pairing potential, J_{ij} represents the period-2 charge order, and Q_{ij} corresponds to the current pattern, which is consistent with the symmetry analysis in Ref. [27]. Also, the distributions of the magnitudes of these order parameters near the vortex have been analyzed and obtained in Fig. 2 (d). Importantly, the electronic Hamiltonian of Eq. (3.1) is explicitly gauge invariant, making it a suitable starting point for our subsequent discussion on the behavior of the electronic spectrum near vortices.

B. Vortex states of Dirac fermions

In the absence of the electromagnetic field, both J_{ij} and Q_{ij} vanish in a homogeneous d -wave superconducting phase. The Hamiltonian in Eq. (3.1) in momentum space can then be expressed as:

$$H_c = \sum_{\mathbf{k}} H_0 c_{\mathbf{k},\sigma}^\dagger c_{\mathbf{k},\sigma} + \sum_{\mathbf{k}} \Delta_{\mathbf{k}} \epsilon_{\alpha\beta} c_{\mathbf{k},\alpha} c_{-\mathbf{k},\beta} + \text{H.c.} \tag{3.5}$$

with $\Delta_{\mathbf{k}} = \Delta_0 \times (-\cos k_x + \cos k_y)$ and $\Delta_0 \equiv 4(1 + \sqrt{2})J^{-1}\Phi^2\gamma^2\Delta$. Notably, the self-energy in $H_0(\omega)$, i.e., $\Sigma(k, \omega) = \Phi^2 / (\omega - \epsilon_{\mathbf{k}}^{f_1})$, is small at the momentum (k_F, k_F) , leading to the approximation $H_0 \simeq \epsilon_{\mathbf{k}}^c$

near $(\pm k_F, \pm k_F)$. For simplicity, the momentum space will be rotated by $\pi/4$:

$$\begin{pmatrix} k_x \\ k_y \end{pmatrix} \rightarrow = \frac{1}{\sqrt{2}} \begin{pmatrix} 1 & -1 \\ 1 & 1 \end{pmatrix} \begin{pmatrix} k_x \\ k_y \end{pmatrix}, \quad (3.6)$$

resulting in the four Dirac points at the following momenta:

$$\mathbf{q}_1 = (\sqrt{2}k_F, 0), \quad \mathbf{q}_2 = (0, \sqrt{2}k_F), \quad \mathbf{q}_3 = (-\sqrt{2}k_F, 0), \quad \mathbf{q}_4 = (0, -\sqrt{2}k_F) \quad (3.7)$$

as depicted in Fig. 3(b). Expanding near each Dirac point \mathbf{q}_α such that $\mathbf{k} = \mathbf{q}_\alpha + \mathbf{p}$, under the Nambu basis $\psi_\alpha(\mathbf{p}) = (c_{\alpha\uparrow}(\mathbf{p}) \ c_{\alpha\downarrow}^\dagger(-\mathbf{p}))^T$, the Hamiltonian in Eq. (3.5) can be rewritten as $H_c = \sum_\alpha \int d^2\mathbf{p} \psi_\alpha^\dagger(\mathbf{p}) h_\alpha(\mathbf{p}) \psi_\alpha(\mathbf{p})$, with $c_{\alpha\sigma}(\mathbf{p}) \equiv c_\sigma(\mathbf{q}_\alpha + \mathbf{p})$, where α denotes the index of the Dirac points. For now, we focus on the node $\alpha = 1$ and postpone the discussion of the other nodes for later. The corresponding Hamiltonian matrix for this Dirac point with $\alpha = 1$ is given by:

$$h_1 = v_F p_x \sigma_z - v_F A_x \sigma_0 + v_\Delta p_y \sigma_x \quad (3.8)$$

where $v_\Delta = \Delta_0 \sqrt{2} k_F$ and $\sigma_x, \sigma_y, \sigma_z$ are Pauli matrices while σ_0 is the unit 2×2 matrix. So far, the complicated ‘Fermi arc’-like electronic behaviors H_0 have been reduced to four free Dirac fermions in the d -wave SC phase. Next, based on this simplified description, we will continue the discussion of vortex physics in the presence of a vortex field.

Based on the analysis in Sec. II B, we established that in the presence of a magnetic field, around the 2π vortex, the d -density wave potential Q_{ij} in Eq. (3.4) always vanishes, while a local charge order potential J_{ij} in Eq. (3.4) is induced. First, we will temporarily ignore the local charge density potential, focusing on the problem of Dirac fermions perceiving a π -flux. In the following calculation, the suppression of the SC order parameter magnitude inside the vortex core will be ignored since the size of the vortex core in cuprates is so small compared to the size of the magnetic halo.

Now, the Franz-Tešanović transformation U acting on the electronic Hamiltonian Eq. (3.5) is applicable here [47–54]:

$$U^{-1} H_c U = \sum_{\mathbf{k}} \begin{pmatrix} e^{-i\Phi_A} \epsilon_{\mathbf{k}-\mathbf{A}}^c e^{i\Phi_A} & e^{-i\Phi_A} e^{i\phi/2} \Delta_{\mathbf{k}} e^{i\phi/2} e^{-i\Phi_B} \\ e^{i\Phi_B} e^{-i\phi/2} \Delta_{\mathbf{k}} e^{-i\phi/2} e^{i\Phi_A} & -e^{-i\Phi_B} \epsilon_{-(\mathbf{k}+\mathbf{A})}^c e^{i\Phi_B} \end{pmatrix} \quad (3.9)$$

$$= \sum_{\mathbf{k}} \begin{pmatrix} \epsilon_{\mathbf{k}-\mathbf{A}+\nabla\Phi_A}^c & \Delta_{\mathbf{k}+\mathbf{A}} \\ \Delta_{\mathbf{k}+\mathbf{A}} & -\epsilon_{-(\mathbf{k}+\mathbf{A}-\nabla\Phi_B)}^c \end{pmatrix} \quad (3.10)$$

where

$$U = \begin{pmatrix} e^{i\Phi_A} & 0 \\ 0 & e^{-i\Phi_B} \end{pmatrix} \quad (3.11)$$

and ϕ in Eq. (3.9) represents the coordinate angle, arising from the 2π superconducting vortex. Here, we assume that $\Phi_A + \Phi_B = \phi$, and the new ‘gauge field’ $\mathcal{A} = (\nabla\Phi_A - \nabla\Phi_B)/2$ in Eq. (3.10) satisfies the relation $\oint dl \cdot \mathcal{A} = \pi$, corresponding to a π -flux vortex completely localized at the origin.

Following this transformation U , the Hamiltonian matrix of Eq. (3.8) can be expressed as:

$$h_1 = v_F (p_x + \mathcal{A}_x) \sigma_z + v_F V_x \sigma_0 + v_\Delta (p_y + \mathcal{A}_y) \sigma_x \quad (3.12)$$

where $\mathbf{V} \equiv (\nabla\Phi_A + \nabla\Phi_B)/2 - \mathcal{A}$ is the Doppler shift of quasiparticle energy due to the background superfluid flow. To obtain an analytic result for vortex physics, this Doppler shift will be ignored in the following discussion, as it was previously shown numerically to result in no qualitative modifications of the analytic results, at least for the case without considering charge order. Then, the length scale can be normalized:

$$x \rightarrow v_F x, \quad y \rightarrow v_\Delta y. \quad (3.13)$$

Following the unitary transformation, the rescaled Hamiltonian matrix of Eq. (3.12) can be expressed as:

$$h_1 = (p_x + a_x) \sigma_x + (p_y + a_y) \sigma_y. \quad (3.14)$$

Switching to polar coordinates,

$$\begin{aligned} p_x &= \cos \phi \left(-i \frac{\partial}{\partial r} \right) - \frac{\sin \phi}{r} \left(-i \frac{\partial}{\partial \phi} \right) \\ p_y &= \sin \phi \left(-i \frac{\partial}{\partial r} \right) + \frac{\cos \phi}{r} \left(-i \frac{\partial}{\partial \phi} \right) \end{aligned} \quad (3.15)$$

and

$$\begin{aligned} a_x &= -\frac{\sin \phi}{2r} \\ a_y &= \frac{\cos \phi}{2r} \end{aligned} \quad (3.16)$$

the Bogoliubov-de Gennes (BdG) equation for $\alpha = 1$ with $q_1 = (k_F, 0)$ takes the form:

$$\begin{pmatrix} 0 & e^{-i\phi} \left[-i \frac{\partial}{\partial r} - \frac{i}{r} \left(-i \frac{\partial}{\partial \phi} + \frac{1}{2} \right) \right] \\ e^{i\phi} \left[-i \frac{\partial}{\partial r} + \frac{i}{r} \left(-i \frac{\partial}{\partial \phi} + \frac{1}{2} \right) \right] & \end{pmatrix} \begin{pmatrix} u(r, \phi) \\ v(r, \phi) \end{pmatrix} = E \begin{pmatrix} u(r, \phi) \\ v(r, \phi) \end{pmatrix}. \quad (3.17)$$

By using the ansatz $u(r, \phi) = e^{i(l-1)\phi} u(r)$ and $v(r, \phi) = e^{il\phi} v(r)$, one obtains the normalized wavefunction with the corresponding energy $E_{q,k} = qk$:

$$\begin{pmatrix} u_{k,l,q,\alpha=1}(r, \phi) \\ v_{k,l,q,\alpha=1}(r, \phi) \end{pmatrix} = \sqrt{\frac{qk}{4\pi}} \begin{pmatrix} e^{i(l-1)\phi} J_{s_l(l-\frac{1}{2})}(kr) \\ s_l i q e^{il\phi} J_{s_l(l+\frac{1}{2})}(kr) \end{pmatrix}. \quad (3.18)$$

where $s_l = \text{sgn}(l)$ with $s_{l=0} = -1$ and J are Bessel functions of the first kind. Here, the states are labeled by three quantum numbers: radial wave vector $k > 0$, angular momentum $l \in \mathbb{Z}$, and $q = \pm$, which characterize the particle and hole branches of excitations.

C. Induced local charging order near the vortex

Next, we will study how the induced local CDW potential J_{ij} influences the electronic spectrum near the vortex. Noting that x -CDW $\rho_{(\pi,0)}$ and y -CDW $\rho_{(0,\pi)}$ are degenerate, we will let $\rho_{(0,\pi)} = 0$ in the following calculation for simplicity. Thus, from Eq. (3.4), the CDW potential in Hamiltonian Eq. (3.1) is given by:

$$\begin{aligned}
& -\frac{\Phi^2}{\gamma^2 J} \sum_{\langle i,j \rangle} \left(J_{ij} c_{i,\sigma}^\dagger c_{j,\sigma} + \text{H.c.} \right) \\
& \approx -\frac{\Phi^2 \gamma^2}{J} (2 + \sqrt{2}) \sum_{\sigma} \sum_{\alpha=1,3} \int d\mathbf{r} \rho_{(\pi,0)}(\mathbf{r}) \left(c_{\alpha,\sigma}^\dagger(\mathbf{r}) c_{\alpha+1,\sigma}(\mathbf{r}) + \text{H.c.} \right) \\
& \approx -\frac{\Phi^2 \gamma^2}{J} (2 + \sqrt{2}) \int d\mathbf{r} \rho_{(\pi,0)}(\mathbf{r}) \int dk' dk \sum_{l,l'} \sum_{q,q'} \sum_{\alpha=1,3} [u_{k',l',q',\alpha}^*(\mathbf{r}) + iv_{k',l',q',\alpha}^*(\mathbf{r})] \\
& \quad \times [u_{k,l,q,\alpha+1}(\mathbf{r}) - iv_{k,l,q,\alpha+1}(\mathbf{r})] \gamma_{k',l',q',\alpha}^\dagger \gamma_{k,l,q,\alpha+1} + \text{h.c.}
\end{aligned} \tag{3.19}$$

where $c_{\alpha,\sigma}$ is the physical electron near the Dirac point with the index α , while γ represents the Bogoliubov quasiparticles characterized by the quantum numbers k, l, q, α , with the corresponding wave function of (u, v) obtained in Eq. (3.18). To ultimately obtain an analytic result, the following approximations are made here:

- The momentum of Dirac points deviates slightly from $(\pm\pi/2, \pm\pi/2)$ as shown in Fig. 3(b), but we will position it exactly at $(\pm\pi/2, \pm\pi/2)$ to let the x -CDW $\rho_{(\pi,0)}$ and y -CDW $\rho_{(0,\pi)}$ potentials connect different Dirac points perfectly.
- We assume that the size of the vortex halo is so large that the CDW potential can be approximately regarded as spatially independent inside the region we are concerned with, i.e., $\rho_{(\pi,0)}(\mathbf{r}) \rightarrow \rho_{(\pi,0)}$, allowing modes with different k to decouple due to the orthogonality relation of Bessel functions.
- The rotational symmetry is broken when the coupling between different Dirac points leads to a coupling term between modes with l and $l \pm 1$. We will neglect the off-diagonal term of l in the following calculation.

Calculations of more realistic situations without these approximations must be done numerically and depend on some microscopic details, i.e., the specific form of spatial decay of the CDW potential. However, we expect that there will be no significant qualitative modifications since the final analytic consequence we obtained mainly arises from the mixture between different flavors of Dirac fermions.

Based on these approximations, we can plug the wavefunction Eq. (3.18) into Eq. (3.19), then the electronic Hamiltonian Eq. (3.1) can be expressed as:

$$H_c = \int_0^\infty dk \sum_l \sum_{\alpha=1,3} \left(\Psi_{k,l}^{(\alpha)} \right)^\dagger V_{k,l}^{(\alpha)} \Psi_{k,l}^{(\alpha)} \quad (3.20)$$

with the basis:

$$\Psi_{k,l}^{(\alpha)} = \left(\gamma_{k,l,q=+,\alpha} \quad \gamma_{k,l,q=+,\alpha+1} \quad \gamma_{k,l,q=-,\alpha} \quad \gamma_{k,l,q=-,\alpha+1} \right)^T \quad (3.21)$$

and the corresponding matrix

$$V_{k,l}^{(\alpha)} = k\sigma_{30} - (\alpha - 2)Fs_l(\sigma_{31} + \sigma_{32} - \sigma_{11} - \sigma_{12}), \quad (3.22)$$

where $\sigma_{ij} = \sigma_i \otimes \tau_j$, with σ and τ being Pauli matrices representing the Dirac point index and particle/hole branch with $q = \pm$, respectively. The parameter $F = -\Phi^2\gamma^2(2 + \sqrt{2})\rho_{(\pi,0)}/4J$ is associated with the CDW potential.

Next, we will calculate the LDOS near the superconducting vortex in the presence of the local charging potential. According to Eq. (3.20), Bogoliubov modes from different Dirac points have an overlap, so the LDOS $\rho(\omega, r)$ can be decomposed into a uniform part $\rho_{\text{uni}}(\omega, r)$ and a modulation part $\rho_{\text{CDW}}(\omega, r)$:

$$\rho(\omega, r) = \rho_{\text{uni}}(\omega, r) + \rho_{\text{CDW}}(\omega, r) \times (-1)^r, \quad (3.23)$$

where the uniform part $\rho_{\text{uni}}(\omega, r)$ comes from the combination of the same Dirac fermions:

$$\rho_{\text{uni}}(\omega, r) \equiv \frac{1}{\pi} \sum_{\sigma} \sum_{\alpha=1}^4 \text{Im} \left\langle c_{\alpha,\sigma}(r) c_{\alpha,\sigma}^\dagger(r) \right\rangle \quad (3.24)$$

and the modulation part $\rho_{\text{CDW}}(\omega, r)$ with the spatial oscillation factor $(-1)^r$ comes from the combination of distinct Dirac fermions:

$$\rho_{\text{CDW}}(\omega, r) \equiv \frac{1}{\pi} \sum_{\sigma} \sum_{\alpha=1,3} \text{Im} \left[\left\langle c_{\alpha,\sigma}(r) c_{\alpha+1,\sigma}^\dagger(r) \right\rangle + \left\langle c_{\alpha+1,\sigma}(r) c_{\alpha,\sigma}^\dagger(r) \right\rangle \right] \quad (3.25)$$

Finally, by combining the electronic Hamiltonian for the Bogoliubov quasiparticles in Eq. (3.20) and the wavefunction of Bogoliubov quasiparticles given in Eq. (3.18), the total density of states Eq. (3.23) is given by:

$$\begin{aligned} \rho(\omega, r) = & \frac{1}{\pi} \frac{|\omega|}{\sqrt{-2F^2 + \omega^2}} \sum_{\sigma=\pm} \left[\frac{4\omega_\sigma}{\pi} \text{Si}(2\omega_\sigma r) + \frac{2 \cos(2\omega_\sigma r)}{\pi r} \right] \\ & \times \left[1 + \text{sgn}(\omega) \frac{(2\sqrt{2}F + \sigma\omega_\sigma)}{\sqrt{2}\sqrt{2F^2 + (\omega_\sigma + \sigma\sqrt{2}F)^2}} (-1)^r \right] \end{aligned} \quad (3.26)$$

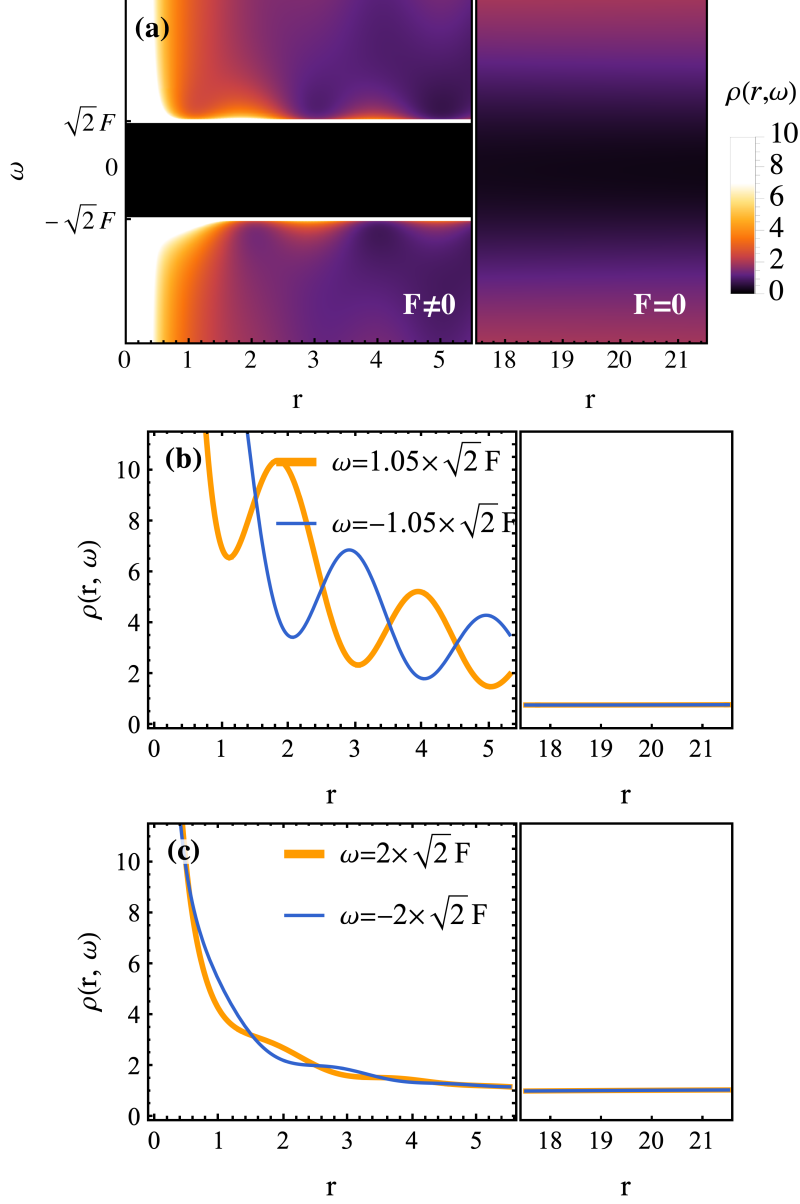


FIG. 4: With the parameters $c = 1/10$ and $F = 0.3$, LDOS $\rho(r, \omega)$ near the vortex from Eq. (3.26) is plotted in the left panel, and $\rho(r, \omega)_\infty$ far from the vortex from Eq. (3.27) is plotted in the right panel, following the substitution $r \rightarrow cr$. (a) Frequency-spatial distribution of LDOS. (b) Spatial dependence of LDOS near the coherence peak around the sub-gap. (c) Spatial dependence of LDOS at frequencies much higher than the coherence peak.

as $\omega^2 > 2F^2$, while $\rho(\omega, r) = 0$ as $\omega^2 < 2F^2$. Here, $\omega_\sigma = -\sigma\sqrt{2F} + \sqrt{-2F^2 + \omega^2}$ and $\text{Si}(x) \equiv \int_0^x \frac{\sin t}{t} dt = \pi \sum_{l \geq 0} J_{l+1/2}^2(x/2)$. This hard gap of $2F$ in this spectrum is an artifact of the assumed exact nesting of the the CDW wavevector with the separation between the nodal points. Note that in our simplified model, the induced charge order interaction only exists around the vortex and completely vanishes far away from the vortex and deep in the homogeneous SC part. In the latter case, the local density of states $\rho_\infty(\omega, r)$

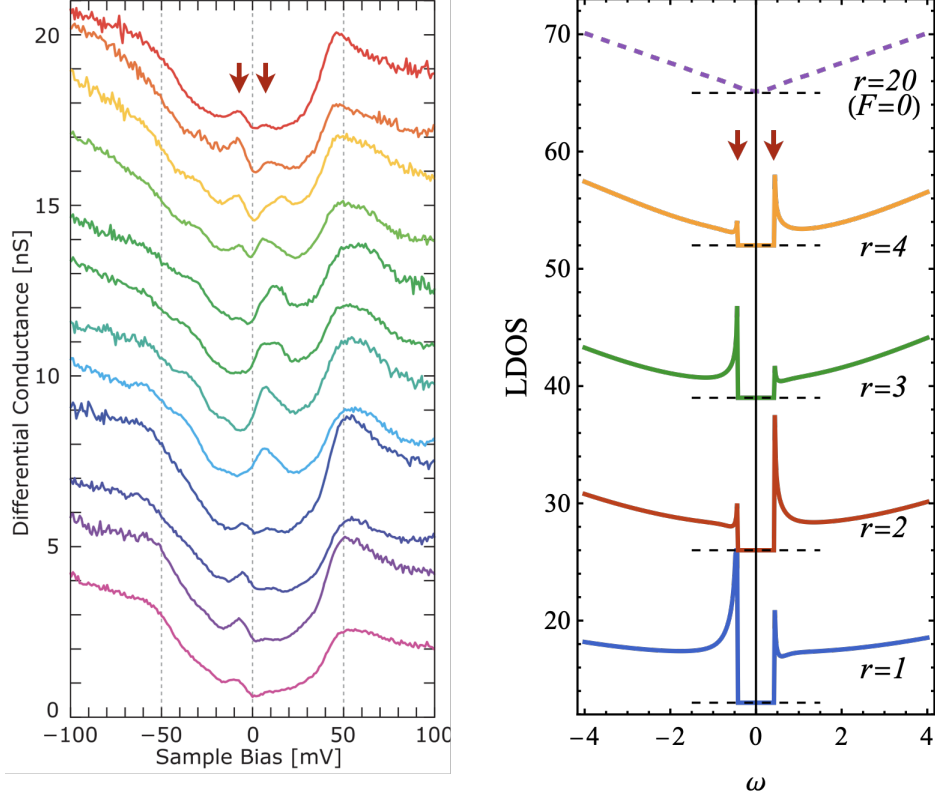


FIG. 5: Left panel: experimental data from STM as reported in Fig. 2(c) of Ref. [5] (red arrows added). Right panel: The total local density of states $\rho(r, \omega)$ in Eq. (3.26) and Eq. (3.27), following the substitution $r \rightarrow cr$. The observed sub-peaks in the STM are indicated with red arrows in both panels.

can be obtained by setting $F = 0$ in Eq. (3.26), resulting in:

$$\rho_{\infty}(\omega, r) \equiv \rho(\omega, r)_{F \rightarrow 0} = \frac{4}{\pi^2} \left[2\omega \text{Si}(2\omega r) + \frac{\cos(2\omega r)}{r} \right] \quad (3.27)$$

which is consistent with the result obtained in Ref. [52, 53]. However, note that the crossover regimes between them depend highly on microscopic details, which is not the focus of this work.

Additionally, the inverse coordinate transformation in Eq. (3.6) and Eq. (3.13) is also needed to fit the actual situation, resulting in $r \rightarrow cr$ along the x direction, where $c \equiv \sqrt{v_F^{-2}/2 + v_{\Delta}^{-2}/2}$, which will be determined phenomenologically in realistic cases.

As a result, the total LDOS spectra after the replacement $r \rightarrow cr$ are shown in Fig. 4, with the left panels corresponding to the physics near the vortex core, as described by Eq. (3.26), and the right panels corresponding to the physics far away from the vortex core, as described by Eq. (3.27). From Fig. 4(a), instead of a zero-bias peak, a gap of magnitude $\sqrt{2}F$ is observed around the vortex at zero frequency, accompanied by a coherent peak at the $\pm\sqrt{2}F$ frequency. This phenomenon originates from the interaction of the CDW potential coupling distinct gapless Dirac points, forming a gap. Note that this is the effective

theory of Dirac points, so the observed sub-gap is actually inside the d -wave SC gap, meaning the SC Bogoliubov peak with higher energy is not shown here. Moreover, compared with the LDOS close to the coherent peak $\pm\sqrt{2}F$ [as shown in Fig. 4(b)] of the sub-gap and far away from such peak [as shown in Fig. 4(c)], one can find that, in proximity to the vortex core, the sub-gap spectrum exhibits apparent spatial modulation with a period of $2a$. More importantly, this modulation exhibits an ‘anti-phase’ behavior for frequencies of opposite signs: this arises from the fact that the charge order induced amplitude for an electron near one Dirac point to convert to a hole near a different Dirac point, given in Eq. (B1) exhibits opposite signs for opposite frequencies, as discussed in Appendix B. Furthermore, far from the vortex core, the density of states exhibits a featureless linear- ω dependency, which is shown in the dashed line of Fig. 5(b), and can be directly obtained via the expansion of Eq. (3.27) at the large r limit. Such a result aligns with the characteristic ‘V’-shape behavior of d -wave superconductors.

Finally, the total local density of states $\rho(r, \omega)$ in Eq. (3.26) and Eq. (3.27) can be compared with the vortex halo observed by STM [3, 5–7] directly, as shown in Fig. 5.

IV. DISCUSSION

Our paper has considered the nature of vortices in a d -wave superconductor obtained by a confinement transition from the pseudogap metal. In terms of broken symmetry, and low energy quasiparticle spectrum, such a superconductor is identical to a d -wave superconductor obtained from a BCS pairing transition of a Fermi liquid with a Luttinger volume Fermi surface [31]. But, as we have shown here, the nature of the pseudogap does reveal itself in the short-distance physics in and around the vortex core.

As is well known, the conventional transition from the Fermi liquid to the d -wave superconductor is described by the Landau-Ginzburg theory of the condensation of a complex scalar field carrying charge $2e$, representing the superconducting order parameter. We have considered here a continuum theory of the pseudogap [27, 33] in which the transition to the d -wave superconductor is described by the condensation of Higgs fields, the 4 charge e complex scalars B_{as} ($s = \pm$ is a valley index, and $a = 1, 2$ is a fundamental SU(2) gauge index), coupled to a SU(2) gauge field. Gauge-invariant bilinears of these Higgs fields realize the d -wave superconducting and period-2 bond density wave order parameters, as shown in Eq. (2.3), and so we can loosely state that the Higgs fields are the ‘square roots’ of the superconducting, charge density wave, and pair density wave order parameters. STM experiments observe LDOS modulations with periods 4 and 8 [3–8, 11–13]. Our theory can be extended to these longer periods [27, 32], either by working with an extended lattice action for the B_{ai} , or by taking the continuum limit with additional valleys and continuum fields. We have left this computationally demanding task for the future, and worked here with

the simpler situation with period 2 density waves for which significant analytic progress has been possible. We also mention earlier work on the vortex structure with 2 complex Higgs fields and a U(1) gauge theory, which did not have charge density wave order parameters [34–37].

Our analysis should be contrasted with numerous earlier studies [11, 14–23] in which the vortex core is described directly in terms of multiple gauge-invariant order parameters, including superconductivity, pair and charge density waves. In such approaches, the normal state above T_c is presumed to be amenable to be a description in a theory of these fluctuating orders. We have instead assumed that the normal state is better described as a FL* metal with a background spin liquid: see Ref. [30] for a description of photoemission and STM in the normal state by such a theory. No symmetry is broken in the FL* state, and there is no direct reference to any particular fluctuating order. The multiple order parameters only make an explicit appearance when we consider the confinement of the spin liquid by the condensation of the Higgs field B .

Our main results appear in Figs. 2(d), 4, and 5(b), along with experimental data in Fig. 5(a). We considered a Higgs potential for B so that the bulk homogeneous ground state is a d -wave superconductor. Nevertheless, as shown in Fig. 2(d), charge order emerges in the vortex core: this is a natural consequence of the associated suppression of superconductivity in the core, and the ability of the Higgs fields to rotate into the charge order direction (a complementary approach to this physics is provided by dual theories of quantum fluctuations of the vortices [38–40]). Figs. 4(a) and 5(b) show the absence of the Wang-Macdonald zero-bias peak, and the associated appearance of peaks at non-zero bias in the vortex core. Finally, and most remarkably, these peaks have spatial modulations which are out-of-phase between positive and negative bias, as seen in Figs. 4(b) and 5(b). This is due to the Dirac structure of the quasiparticles in the d -wave superconductor, and matches the observations of Matsuba *et al.* [5], which we show in Fig. 5(a).

Looking ahead, it is clearly important to extend this work to spatial modulations with longer periods, and understand the connection to models used for quantum oscillations [32]. As we have noted earlier, the spatial modulations of the Higgs fields appear both in Δ_{ij} and ρ_i (see Eq. (1.1)), and this can help understand the relative roles of charge and pair density wave order. Finally, a significant experimental and theoretical challenge is to understand the evolution of the vortex structure from low to high doping, as one proceeds from the parent pseudogap metal to the parent Fermi liquid [28, 43].

Acknowledgements

We thank Pietro Bonetti, Maine Christos, Seamus Davis, Peter Hirschfeld and Steve Kivelson for valuable discussions. This research was supported by the U.S. National Science Foundation grant No. DMR-2245246 and by the Simons Collaboration on Ultra-Quantum Matter which is a grant from the Simons Foundation (651440, S.S.). J.-X. Z. acknowledges the support from NSFC (Grant No. 12347107) and the Tsinghua Visiting Doctoral Students Foundation.

Appendix A: Self-consistent calculation of B field

In this section, we will provide more details about the determination of the spatial modulation function in the ansatz for the chargin B at the continuum limit, as shown in Sec. II.

1. Flat configuration

With the flat configuration of \mathbf{a}^z , the ansatz for the chargin B is given by Eq. (2.5). The free energy, derived by plugging this ansatz into Eq. (2.2), is given by:

$$F = \int_0^\infty dr 2rb^2 \left[\frac{\partial f(r)}{\partial r} \right]^2 + b^2 \frac{f^2(r)}{r} \left[1 + \frac{\Phi_A(r)}{2\pi} \right]^2 + b^2 \frac{f^2(r)}{r} \left[1 + \frac{\Phi_A(r)}{2\pi} \right]^2 + 2mrb^2 f^2(r) + (4u + v_3)rb^4 f^4(r) + \frac{1}{g} \frac{1}{r} \left(\frac{\partial}{\partial r} \Phi_A(r) \right)^2 \quad (\text{A1})$$

where $f(r) \in [0, 1]$ and ϕ is the angle in real space (as illustrated in Fig. 6), encircling the pole. The equations of motion derived from Eq. (A1) are:

$$-2 \frac{\partial f(r)}{\partial r} - 2r \frac{\partial^2 f(r)}{\partial r^2} + \frac{f(r)}{r} \left[1 + \frac{\Phi_A(r)}{2\pi} \right]^2 + \frac{f(r)}{r} \left[1 + \frac{\Phi_A(r)}{2\pi} \right]^2 + 2mr f(r) + 2(4u + v_3)rb^2 f^3(r) = 0 \quad (\text{A2})$$

$$2b^2 \frac{rf^2(r)}{2\pi} \left[n_+ + \frac{\Phi_A(r)}{2\pi} \right] + 2b^2 \frac{rf^2(r)}{2\pi} \left[n_- + \frac{\Phi_A(r)}{2\pi} \right] + \frac{2}{g} \frac{\partial}{\partial r} \Phi(r) - \frac{2r}{g} \frac{\partial^2 \Phi(r)}{\partial r^2} = 0 \quad (\text{A3})$$

with the boundary conditions:

$$\begin{aligned} f(r) &\xrightarrow{r \rightarrow 0} 0, & f(r) &\xrightarrow{r \rightarrow \infty} 1 \\ \Phi_A(r) &\xrightarrow{r \rightarrow 0} 0, & \Phi_A(r) &\xrightarrow{r \rightarrow \infty} 2\pi. \end{aligned} \quad (\text{A4})$$

The numerical results derived from Eq. (A2) and Eq. (A3) under the boundary conditions Eq. (A4) are depicted in Fig. 2(a).

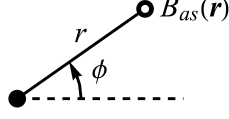


FIG. 6: The schematic diagram of r and ϕ in Eq. (2.5).

2. Vison-like configuration

Similarly, with the vison-like configuration of \mathbf{a}^z , the ansatz for the chargon B is given by Eq. (2.8).

The free energy, derived by plugging this ansatz into Eq. (2.2), is given by:

$$\begin{aligned}
F = & \int_0^\infty dr b^2 r \left[\frac{\partial f(r)}{\partial r} \right]^2 + b^2 r \left[\frac{\partial h(r)}{\partial r} \right]^2 + b^2 r \frac{f^2(r)}{r^2} \left[-1 + \frac{\Phi_A(r)}{2\pi} + \frac{\Phi_a(r)}{2\pi} \right]^2 + b^2 r \frac{h^2(r)}{r^2} \left[\frac{\Phi_A(r)}{2\pi} - \frac{\Phi_a(r)}{2\pi} \right]^2 \\
& + b^2 r m (f^2(r) + h^2(r)) + b^4 r u (f^2(r) + h^2(r))^2 + v_1 b^4 r [f^2(r) - h^2(r)]^2 + v_3 b^4 r f^2(r) h^2(r) \frac{\partial f(r)}{\partial r} \quad (\text{A5}) \\
& + \frac{1}{g} \frac{1}{r} \left(\frac{\partial \Phi_A(r)}{\partial r} \right)^2 + \frac{1}{\lambda} \frac{1}{r} \left(\frac{\partial \Phi_a(r)}{\partial r} \right)^2
\end{aligned}$$

The corresponding equations of motion are:

$$\begin{aligned}
-\frac{1}{r} \frac{\partial f(r)}{\partial r} - \frac{\partial^2 f(r)}{\partial r^2} + \frac{f(r)}{r^2} \left[-1 + \frac{\Phi_A(r)}{2\pi} + \frac{\Phi_a(r)}{2\pi} \right]^2 + m f(r) + 2b^2 u (f^2(r) + h^2(r)) f(r) \\
+ 2v_1 b^2 [f^2(r) - h^2(r)] f(r) + v_3 b^2 f(r) h^2(r) = 0 \quad (\text{A6})
\end{aligned}$$

$$\begin{aligned}
-\frac{1}{r} \frac{\partial h(r)}{\partial r} - \frac{\partial^2 h(r)}{\partial r^2} + \frac{h(r)}{r^2} \left[\frac{\Phi_A(r)}{2\pi} - \frac{\Phi_a(r)}{2\pi} \right]^2 + m h(r) + 2b^2 u (f^2(r) + h^2(r)) h(r) \\
- 2v_1 b^2 [f^2(r) - h^2(r)] h(r) + v_3 b^2 h(r) f^2(r) = 0 \quad (\text{A7})
\end{aligned}$$

$$\frac{b^2 r}{2\pi} f^2(r) \left[-1 + \frac{\Phi_A(r)}{2\pi} + \frac{\Phi_a(r)}{2\pi} \right] - \frac{b^2 r}{2\pi} h^2(r) \left[\frac{\Phi_A(r)}{2\pi} - \frac{\Phi_a(r)}{2\pi} \right] + \frac{1}{\lambda} \frac{\partial \Phi_a(r)}{\partial r} - \frac{r}{\lambda} \frac{\partial^2 \Phi_a(r)}{\partial r^2} = 0 \quad (\text{A8})$$

$$\frac{b^2 r}{2\pi} f^2(r) \left[-1 + \frac{\Phi_A(r)}{2\pi} + \frac{\Phi_a(r)}{2\pi} \right] + \frac{b^2 r}{2\pi} h^2(r) \left[\frac{\Phi_A(r)}{2\pi} - \frac{\Phi_a(r)}{2\pi} \right] + \frac{1}{g} \frac{\partial \Phi_A(r)}{\partial r} - \frac{r}{g} \frac{\partial^2 \Phi_A(r)}{\partial r^2} = 0 \quad (\text{A9})$$

with the boundary conditions:

$$\begin{aligned}
f(r) & \xrightarrow{r \rightarrow 0} 0, & f(r) & \xrightarrow{r \rightarrow \infty} 1, \\
h(r) & \xrightarrow{r \rightarrow 0} h_0, & h(r) & \xrightarrow{r \rightarrow \infty} 1 \\
\Phi_A(r) & \xrightarrow{r \rightarrow 0} 0, & \Phi_A(r) & \xrightarrow{r \rightarrow \infty} \pi, \\
\Phi_a(r) & \xrightarrow{r \rightarrow 0} 0, & \Phi_a(r) & \xrightarrow{r \rightarrow \infty} \pi.
\end{aligned} \quad (\text{A10})$$

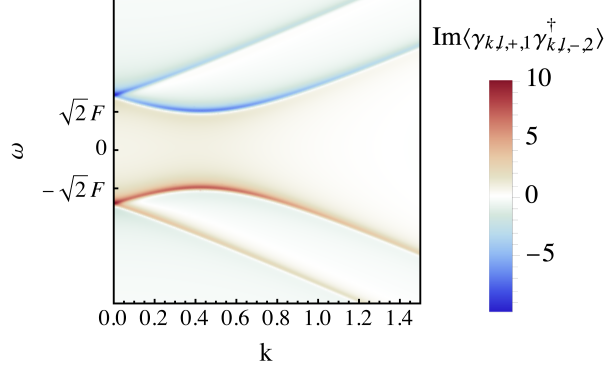


FIG. 7: With parameters $F = 0.3$ and $\Gamma = 0.03$, the imaginary part of $\langle \gamma_{k,l,+1} \gamma_{k,l,-2}^\dagger \rangle$ for $l > 0$ from Eq. (B1) after the replacement of $\omega \rightarrow \omega + i\Gamma$.

The value b can be deduced from Eq. (A6) in the large r limit, resulting in $b^2 = \frac{-m}{(4u+v)}$. Also, h_0 is set such that $\partial_r h(r) \xrightarrow{r \rightarrow 0} 0$. The numerical results derived from Eqs. (A6)-(A9) under the boundary conditions Eq. (A10) are shown in Fig. 2(c).

Appendix B: Derivation of LDOS Near the Vortex

In this section, we will provide more details about the determination of LDOS $\rho(\omega, r)$ in Eq. (3.26).

Firstly, based on the electronic Hamiltonian Eq. (3.20), the Green's function of Bogoliubov quasiparticles γ is given by:

$$\left\langle \Psi_{k,l}^{(\alpha)} \otimes \left(\Psi_{k,l}^{(\alpha)} \right)^\dagger \right\rangle = - \left(\omega - V_{k,l}^{(\alpha)} \right)^{-1} = \frac{M^{(\alpha)}}{16F^4 - 8F^2\omega^2 + (k^2 - \omega^2)^2} \quad (\text{B1})$$

where $\alpha = 1, 3$ and $M^{(\alpha)}$ represents a 4×4 matrix with the expression:

$$\begin{aligned} M^{(\alpha)} = & 4F^2 (\omega\sigma_{00} + k\sigma_{10}) + (k^2 - \omega^2) (\omega\sigma_{00} + k\sigma_{30}) - (\alpha - 2)Fs_l (4F^2 - \omega^2) (-\sigma_{11} - \sigma_{12} + \sigma_{31} + \sigma_{32}) \\ & + (\alpha - 2)Fs_l (2k\omega (\sigma_{01} + \sigma_{02}) + k^2 (\sigma_{11} + \sigma_{12} + \sigma_{31} + \sigma_{32})) \end{aligned} \quad (\text{B2})$$

Here, we present the imaginary part of $\langle \gamma_{k,l,+1} \gamma_{k,l,-2}^\dagger \rangle$, which corresponds to the amplitude for an electron near the $\alpha = 1$ Dirac point converting to a hole near the $\alpha = 2$ Dirac point, in Fig. 7 as an example. The sign of the amplitude is opposite for opposite frequencies, and all the weight is inside the gap $-\sqrt{2}F < \omega < \sqrt{2}F$.

Starting from Eq. (3.23), the LDOS $\rho(\omega, r)$ is contributed by both the uniform part $\rho_{\text{uni}}(\omega, r)$ and the modulation part $\rho_{\text{CDW}}(\omega, r)$. In the following, we will discuss these two parts of the contribution separately.

	$\omega > \sqrt{2F}$	$\omega < \sqrt{2F}$
$\sqrt{2F} + \sqrt{\omega^2 - 2F^2}$	+	-
$\sqrt{2F} - \sqrt{\omega^2 - 2F^2}$	-	-
$-\sqrt{2F} + \sqrt{\omega^2 - 2F^2}$	+	+
$-\sqrt{2F} - \sqrt{\omega^2 - 2F^2}$	-	-

TABLE III: The sign of $\pm\sqrt{2F} \pm \sqrt{-2F^2 + \omega^2}$ in different regions of ω

Using the wavefunction of Bogoliubov quasiparticles given in Eq. (3.18), the uniform part $\rho_{\text{uni}}(\omega, r)$ can be further expressed as:

$$\begin{aligned}
\rho_{\text{uni}}(\omega, r) &= \frac{2}{\pi} \sum_{\alpha=1}^4 \text{Im} \left\langle c_{\alpha, \uparrow}(r) c_{\alpha, \uparrow}^\dagger(r) \right\rangle \\
&= \frac{2}{\pi} \sum_{\alpha=1}^4 \int_0^\infty dk \sum_l \sum_{q, q'=\pm} [u_{k, l, q, \alpha}(r) - i v_{k, l, q, \alpha}(r)] [u_{k, l, q', \alpha}^*(r) + i v_{k, l, q', \alpha}^*(r)] \text{Im} \left\langle \gamma_{k, l, q, \alpha} \gamma_{k, l, q', \alpha}^\dagger \right\rangle \\
&= \frac{2}{\pi^2} \int_0^\infty dk \sum_l \left[4 \sum_{l \geq 0} J_{l+1/2}^2(kr) + \frac{2 \cos(2kr)}{\pi kr} \right] \sum_{\sigma_1, \sigma_2=\pm} \text{Im} \frac{-k}{2 \left(\omega + i0^+ - \sigma_1 \sqrt{2F^2 + (k + \sigma_2 \sqrt{2F})^2} \right)} \\
&= \frac{2}{\pi} \int_0^\infty dk \left[\frac{2k}{\pi} \text{Si}(2kr) + \frac{1 \cos(2kr)}{\pi r} \right] \sum_{\sigma_1, \sigma_2=\pm} \delta \left(\omega - \sigma_1 \sqrt{2F^2 + (k + \sigma_2 \sqrt{2F})^2} \right) \quad (\text{B3})
\end{aligned}$$

where $\left\langle \gamma_{k, l, q, \alpha} \gamma_{k, l, q', \alpha}^\dagger \right\rangle$ can be obtained from Eq. (B1).

According to the relation $\delta[g(x)] = \sum_i \frac{\delta(x-x_i)}{|g'(x_i)|}$, where x_i denotes the roots of g , the following equation can be derived:

$$\delta \left(\omega \pm \sqrt{2F^2 + (k + \sigma \sqrt{2F})^2} \right) = \left| \frac{\omega}{\sqrt{2F^2 + \omega^2}} \right| \sum_{\sigma'=\pm} \delta \left(k - \left(-\sigma \sqrt{2F} + \sigma' \sqrt{-2F^2 + \omega^2} \right) \right). \quad (\text{B4})$$

By referring to Table III, which illustrates the signs of $\pm\sqrt{2F} \pm \sqrt{-2F^2 + \omega^2}$, we can analyze the values of $\rho_{\text{uni}}(\omega, r)$ within different regions of ω . In the case of $\omega > \sqrt{2F}$,

$$\sum_{\sigma_1, \sigma_2=\pm} \delta \left(\omega - \sigma_1 \sqrt{2F^2 + (k + \sigma_2 \sqrt{2F})^2} \right) = \sum_{\sigma=\pm} \left| \frac{\omega}{\sqrt{-2F^2 + \omega^2}} \right| \delta \left(k - \left(-\sigma \sqrt{2F} + \sqrt{-2F^2 + \omega^2} \right) \right) \quad (\text{B5})$$

Consequently, the expression for $\rho_{\text{uni}}(\omega, r)$ in Eq. (B3) is:

$$\rho_{\text{uni}}(\omega, r) = \frac{1}{\pi} \left| \frac{\omega}{\sqrt{-2F^2 + \omega^2}} \right| \sum_{\sigma=\pm} \left[\frac{4\omega_\sigma}{\pi} \text{Si}(2\omega_\sigma r) + \frac{2 \cos(2\omega_\sigma r)}{\pi r} \right] \quad (\text{B6})$$

where

$$\omega_\sigma \equiv -\sigma \sqrt{2F} + \sqrt{\omega^2 - 2F^2}. \quad (\text{B7})$$

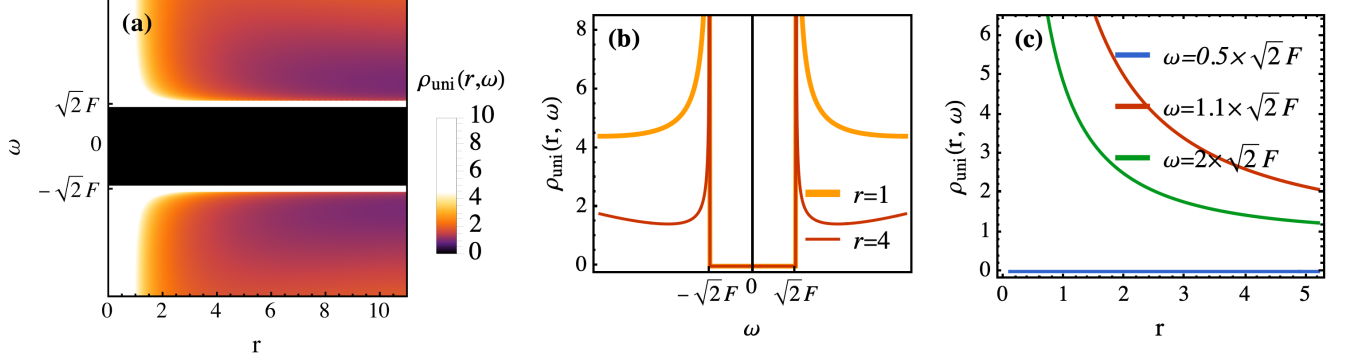


FIG. 8: The uniform component of the local density of states $\rho_{\text{uni}}(r, \omega)$ in Eq. (B10), following the substitution $r \rightarrow cr$. This is considered with the parameters $c = 1/10$ and $F = 0.3$.

In the scenario where $\omega < \sqrt{2}F$, a similar approach leads to the conclusion that $\rho_{\text{uni}}(\omega, r)$ remains as defined in the above equation. However, for $-\sqrt{2}F < \omega < \sqrt{2}F$, $\omega - \sigma_1 \sqrt{2F^2 + (k + \sigma_2 \sqrt{2}F)^2} \neq 0$ consistently, implying that:

$$\sum_{\sigma_1, \sigma_2 = \pm} \delta \left(\omega - \sigma_1 \sqrt{2F^2 + (k + \sigma_2 \sqrt{2}F)^2} \right) = 0, \quad (\text{B8})$$

and therefore,

$$\rho_{\text{uni}}(\omega, r) = 0 \quad (\text{B9})$$

As a result, $\rho_{\text{uni}}(\omega, r)$ can be formulated as:

$$\rho_{\text{uni}}(\omega, r) = \begin{cases} \frac{1}{\pi} \left| \frac{\omega}{\sqrt{-2F^2 + \omega^2}} \right| \sum_{\sigma = \pm} \left[\frac{4\omega_{\sigma}}{\pi} \text{Si}(2\omega_{\sigma}r) + \frac{2}{\pi} \frac{\cos(2\omega_{\sigma}r)}{r} \right] & \omega^2 > 2F^2 \\ 0 & \omega \leq 2F^2 \end{cases}. \quad (\text{B10})$$

The results of Eq. (B10) after substituting $r \rightarrow cr$, are depicted in Fig. 8. This illustration suggests the opening of a gap with a magnitude of $\sqrt{2}F$, leading to a coherent peak at the frequency $\sqrt{2}F$. Notably, LDOS exhibits a tendency towards divergence as it approaches the vortex core.

On the other hand, the modulation part $\rho_{\text{CDW}}(\omega, r)$ can be further given by:

$$\begin{aligned} \rho_{\text{CDW}}(\omega, r) &= \frac{2}{\pi} \text{Im} \left[\langle c_{1,\sigma}(r) c_{2,\sigma}^{\dagger}(r) \rangle + 1 \leftrightarrow 2 + \langle c_{3,\sigma}(r) c_{4,\sigma}^{\dagger}(r) \rangle + 3 \leftrightarrow 4 \right] \\ &= \frac{2}{\pi^2} \int_0^{\infty} dk \left[\frac{4}{\pi} \text{Si}(2kr) + \frac{2}{\pi} \frac{\cos(2kr)}{kr} \right] \text{Im} \frac{4Fk(4F^2 - v^2)}{\prod_{\sigma_1, \sigma_2 = \pm} \left(\omega + i0^+ - \sigma_1 \sqrt{2F^2 + (k + \sigma_2 \sqrt{2}F)^2} \right)} \\ &= -\frac{1}{\pi} \int_0^{\infty} dk \left[\frac{4k}{\pi} \text{Si}(2kr) + \frac{2}{\pi} \frac{\cos(2kr)}{r} \right] \sum_{\sigma_1, \sigma_2 = \pm} \frac{(2\sqrt{2}F + \sigma_1 k)}{\sqrt{2} \sqrt{2F^2 + (k + \sigma_1 \sqrt{2}F)^2}} \sigma_2 \\ &\quad \times \delta \left(\omega + \sigma_2 \sqrt{2F^2 + (k + \sigma_1 \sqrt{2}F)^2} \right) \end{aligned} \quad (\text{B11})$$

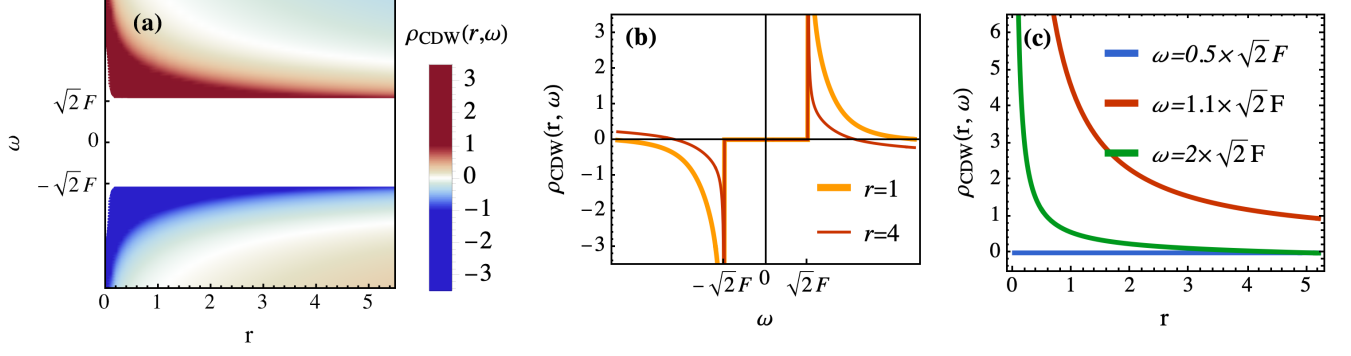


FIG. 9: The charge modulation component of the local density of states $\rho_{\text{CDW}}(r, \omega)$ in Eq. (B19), following the substitution $r \rightarrow cr$. This is considered with the parameters $c = 1/10$ and $F = 0.3$.

From Eq. (B4) and Table III, we can discuss the value of $\rho_{\text{CDW}}(\omega, r)$ at different ω regions. Specifically, when $\omega > \sqrt{2}F$,

$$\begin{aligned} & \sum_{\sigma_1, \sigma_2 = \pm} \frac{(2\sqrt{2}F + \sigma_1 k)}{\sqrt{2}\sqrt{2F^2 + (k + \sigma_1\sqrt{2}F)^2}} \sigma_2 \delta\left(\omega + \sigma_2 \sqrt{2F^2 + (k + \sigma_1\sqrt{2}F)^2}\right) \\ &= - \sum_{\sigma_1 = \pm} \frac{(2\sqrt{2}F + \sigma_1 k)}{\sqrt{2}\sqrt{2F^2 + (k + \sigma_1\sqrt{2}F)^2}} \times \left| \frac{\omega}{\sqrt{-2F^2 + \omega^2}} \right| \delta\left(k - \left(-\sigma_1\sqrt{2}F + \sqrt{-2F^2 + \omega^2}\right)\right) \end{aligned} \quad (\text{B12})$$

thus,

$$\rho_{\text{CDW}}(\omega, r) = \frac{1}{\pi} \sum_{\sigma = \pm} \left[\frac{4\omega_\sigma}{\pi} \text{Si}(2\omega_\sigma r) + \frac{2 \cos(2\omega_\sigma r)}{\pi r} \right] \frac{(2\sqrt{2}F + \sigma\omega_\sigma)}{\sqrt{2}\sqrt{2F^2 + (\omega_\sigma + \sigma\sqrt{2}F)^2}} \frac{|\omega|}{\sqrt{-2F^2 + \omega^2}} \quad (\text{B13})$$

where

$$\omega_\sigma = -\sigma\sqrt{2}F + \sqrt{-2F^2 + \omega^2} \quad (\text{B14})$$

When $\omega < \sqrt{2}F$,

$$\begin{aligned} & \sum_{\sigma_1, \sigma_2 = \pm} \frac{(2\sqrt{2}F + \sigma_1 k)}{\sqrt{2}\sqrt{2F^2 + (k + \sigma_1\sqrt{2}F)^2}} \sigma_2 \delta\left(\omega + \sigma_2 \sqrt{2F^2 + (k + \sigma_1\sqrt{2}F)^2}\right) \\ &= \sum_{\sigma_1 = \pm} \frac{(2\sqrt{2}F + \sigma_1 k)}{\sqrt{2}\sqrt{2F^2 + (k + \sigma_1\sqrt{2}F)^2}} \times \left| \frac{\omega}{\sqrt{-2F^2 + \omega^2}} \right| \delta\left(k - \left(-\sigma_1\sqrt{2}F + \sqrt{-2F^2 + \omega^2}\right)\right) \end{aligned} \quad (\text{B15})$$

thus,

$$\rho_{\text{CDW}}(\omega, r) = -\frac{1}{\pi} \sum_{\sigma = \pm} \left[\frac{4\omega_\sigma}{\pi} \text{Si}(2\omega_\sigma r) + \frac{2 \cos(2\omega_\sigma r)}{\pi r} \right] \frac{(2\sqrt{2}F + \sigma\omega_\sigma)}{\sqrt{2}\sqrt{2F^2 + (\omega_\sigma + \sigma\sqrt{2}F)^2}} \frac{|\omega|}{\sqrt{-2F^2 + \omega^2}} \quad (\text{B16})$$

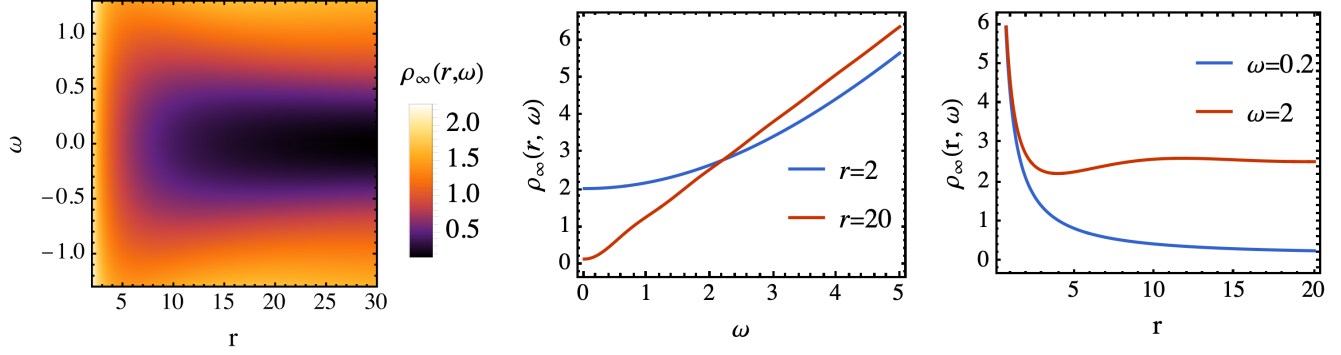


FIG. 10: Local density of states without charge order potential, $\rho_{\text{LDOS}}(r, \omega)$, in Eq. (B21) with the substitution $r \rightarrow cr$. Parameters: $c = 1/10$.

When $-\sqrt{2F} < \omega < \sqrt{2F}$, $\omega - \sigma_1 \sqrt{2F^2 + (k + \sigma_2 \sqrt{2F})^2} \neq 0$ all the time, so that

$$\sum_{\sigma_1, \sigma_2 = \pm} \delta \left(\omega - \sigma_1 \sqrt{2F^2 + (k + \sigma_2 \sqrt{2F})^2} \right) = 0, \quad (\text{B17})$$

yielding

$$\rho_{\text{CDW}}(\omega, r) = 0 \quad (\text{B18})$$

As a result, the expression for $\rho_{\text{CDW}}(\omega, r)$ can be summarized as:

$$\rho_{\text{CDW}}(\omega, r) = \begin{cases} \frac{1}{\pi} \left| \frac{\omega}{\sqrt{-2F^2 + \omega^2}} \right| \sum_{\sigma = \pm} \left[\frac{4\omega_{\sigma}}{\pi} \text{Si}(2\omega_{\sigma}r) + \frac{2}{\pi} \frac{\cos(2\omega_{\sigma}r)}{r} \right] \frac{\text{sgn}(\omega)(2\sqrt{2F} + \sigma\omega_{\sigma})}{\sqrt{2}\sqrt{2F^2 + (\omega_{\sigma} + \sigma\sqrt{2F})^2}} & \text{as } \omega^2 > 2F^2 \\ 0 & \text{as } \omega^2 \leq 2F^2 \end{cases} \quad (\text{B19})$$

where

$$\omega_{\sigma} = -\sigma\sqrt{2F} + \sqrt{-2F^2 + \omega^2} \quad (\text{B20})$$

The result of Eq. (B19) after the substitution $r \rightarrow cr$ is shown in Fig. 9, indicating that coherent peaks at the frequency $\sqrt{2F}$ exhibit opposite signs. Note that the formation of a peak is associated with the formation of a gap, while the opposite sign arises from the opposite amplitude for an electron converting to a hole at distinct Dirac points for opposite frequency, as illustrated in Fig. 7. Such opposite signs of amplitude, combined with the modulation factor $(-1)^r$ in Eq. (3.23), lead to the out-of-phase modulation between positive and negative frequencies.

Combining the results of ρ_{uni} in Eq. (B10) and ρ_{CDW} in Eq. (B19), one obtains the LDOS ρ in Eq. (3.26).

On the other hand, the LDOS without the charge order potential can be obtained by setting $F = 0$, which leads to

$$\rho_{\infty}(\omega, r) \equiv \rho(\omega, r)_{F \rightarrow 0} = \frac{4}{\pi^2} \left[2\omega \text{Si}(2\omega r) + \frac{\cos(2\omega r)}{r} \right], \quad (\text{B21})$$

as in Eq. (3.27). The result of Eq. (B21) is shown in Fig. 10, indicating the enhancement of density as it approaches the vortex core ($r \rightarrow 0$), while there is no significant peak at zero bias. Importantly, far from the vortex core, the LDOS exhibits a linear dependence on frequency, which is characteristic of d -wave superconductors.

-
- [1] C. C. Tsuei and J. R. Kirtley, *Pairing symmetry in cuprate superconductors*, *Rev. Mod. Phys.* **72**, 969 (2000).
 - [2] A. Damascelli, Z. Hussain, and Z.-X. Shen, *Angle-resolved photoemission studies of the cuprate superconductors*, *Rev. Mod. Phys.* **75**, 473 (2003).
 - [3] J. E. Hoffman, E. W. Hudson, K. M. Lang, V. Madhavan, H. Eisaki, S. Uchida, and J. C. Davis, *A Four Unit Cell Periodic Pattern of Quasi-Particle States Surrounding Vortex Cores in $\text{Bi}_2\text{Sr}_2\text{CaCu}_2\text{O}_{8+\delta}$* , *Science* **295**, 466 (2002), [arXiv:cond-mat/0201348 \[cond-mat.supr-con\]](#).
 - [4] G. Levy, M. Kugler, A. A. Manuel, Ø. Fischer, and M. Li, *Fourfold Structure of Vortex-Core States in $\text{Bi}_2\text{Sr}_2\text{CaCu}_2\text{O}_{8+\delta}$* , *Phys. Rev. Lett.* **95**, 257005 (2005), [arXiv:cond-mat/0503219 \[cond-mat.supr-con\]](#).
 - [5] K. Matsuba, S. Yoshizawa, Y. Mochizuki, T. Mochiku, K. Hirata, and N. Nishida, *Anti-phase Modulation of Electron- and Hole-like States in Vortex Core of $\text{Bi}_2\text{Sr}_2\text{CaCu}_2\text{O}_x$ Probed by Scanning Tunneling Spectroscopy*, *Journal of the Physical Society of Japan* **76**, 063704 (2007), [arXiv:0708.4336 \[cond-mat.supr-con\]](#).
 - [6] S. Yoshizawa, T. Koseki, K. Matsuba, T. Mochiku, K. Hirata, and N. Nishida, *High-Resolution Scanning Tunneling Spectroscopy of Vortex Cores in Inhomogeneous Electronic States of $\text{Bi}_2\text{Sr}_2\text{CaCu}_2\text{O}_x$* , *Journal of the Physical Society of Japan* **82**, 083706 (2013), [arXiv:1307.4178 \[cond-mat.supr-con\]](#).
 - [7] T. Machida, Y. Kohsaka, K. Matsuo, K. Iwaya, T. Hanaguri, and T. Tamegai, *Bipartite electronic superstructures in the vortex core of $\text{Bi}_2\text{Sr}_2\text{CaCu}_2\text{O}_{8+\delta}$* , *Nature Communications* **7**, 11747 (2016), [arXiv:1508.00621 \[cond-mat.supr-con\]](#).
 - [8] S. D. Edkins, A. Kostin, K. Fujita, A. P. Mackenzie, H. Eisaki, S. Uchida, S. Sachdev, M. J. Lawler, E. A. Kim, J. C. Séamus Davis, and M. H. Hamidian, *Magnetic field-induced pair density wave state in the cuprate vortex halo*, *Science* **364**, 976 (2019), [arXiv:1802.04673 \[cond-mat.supr-con\]](#).
 - [9] Y. Wang and A. H. MacDonald, *Mixed-state quasiparticle spectrum for d -wave superconductors*, *Phys. Rev. B* **52**, R3876 (1995), [arXiv:cond-mat/9505142 \[cond-mat\]](#).
 - [10] T. Gazdić, I. Maggio-Aprile, G. Gu, and C. Renner, *Wang-MacDonald d -Wave Vortex Cores Observed in Heavily Overdoped $\text{Bi}_2\text{Sr}_2\text{CaCu}_2\text{O}_{8+\delta}$* , *Physical Review X* **11**, 031040 (2021), [arXiv:2103.05994 \[cond-mat.supr-con\]](#).
 - [11] P. Choubey, S. H. Joo, K. Fujita, Z. Du, S. D. Edkins, M. H. Hamidian, H. Eisaki, S. Uchida, A. P. Mackenzie, J. Lee, J. C. S. Davis, and P. J. Hirschfeld, *Atomic-scale electronic structure of the cuprate pair density wave state coexisting with superconductivity*, *Proceedings of the National Academy of Science* **117**, 14805 (2020), [arXiv:2002.11654 \[cond-mat.supr-con\]](#).
 - [12] Z. Du, H. Li, S. H. Joo, E. P. Donoway, J. Lee, J. C. S. Davis, G. Gu, P. D. Johnson, and K. Fujita, *Imaging the energy gap modulations of the cuprate pair-density-wave state*, *Nature (London)* **580**, 65 (2020), [arXiv:2109.14033 \[cond-mat.supr-con\]](#).
 - [13] S. Wang, P. Choubey, Y. X. Chong, W. Chen, W. Ren, H. Eisaki, S. Uchida, P. J. Hirschfeld, and J. C. S. Davis, *Scattering interference signature of a pair density wave state in the cuprate pseudogap phase*, *Nature Communications* **12**, 6087 (2021), [arXiv:2105.06518 \[cond-mat.supr-con\]](#).
 - [14] J.-X. Zhu and C. S. Ting, *Quasiparticle States at a d -Wave Vortex Core in High- T_c Superconductors: Induction of Local Spin Density Wave Order*, *Phys. Rev. Lett.* **87**, 147002 (2001), [arXiv:cond-mat/0105417 \[cond-mat.supr-con\]](#).
 - [15] Y. Zhang, E. Demler, and S. Sachdev, *Competing orders in a magnetic field: Spin and charge order in the cuprate superconductors*, *Phys. Rev. B* **66**, 094501 (2002), [arXiv:cond-mat/0112343 \[cond-mat.str-el\]](#).
 - [16] H. Tsuchiura, M. Ogata, Y. Tanaka, and S. Kashiwaya, *Electronic states around a vortex core in high- T_c superconductors based on the t - J model*, *Phys. Rev. B* **68**, 012509 (2003), [arXiv:cond-mat/0302030 \[cond-](#)

[mat.supr-con](#)].

- [17] Y. Chen, Z. D. Wang, and C. S. Ting, *Temperature dependence of vortex charges in high-temperature superconductors*, *Phys. Rev. B* **67**, 220501 (2003), [arXiv:cond-mat/0302555](#) [[cond-mat.supr-con](#)].
- [18] L. Balents, L. Bartosch, A. Burkov, S. Sachdev, and K. Sengupta, *Putting competing orders in their place near the Mott transition*, *Phys. Rev. B* **71**, 144508 (2005), [arXiv:cond-mat/0408329](#) [[cond-mat.str-el](#)].
- [19] M. Schmid, B. M. Andersen, A. P. Kampf, and P. J. Hirschfeld, *d-Wave superconductivity as a catalyst for antiferromagnetism in underdoped cuprates*, *New Journal of Physics* **12**, 053043 (2010).
- [20] D. F. Agterberg and J. Garaud, *Checkerboard order in vortex cores from pair-density-wave superconductivity*, *Phys. Rev. B* **91**, 104512 (2015), [arXiv:1412.5101](#) [[cond-mat.supr-con](#)].
- [21] Y. Wang, S. D. Edkins, M. H. Hamidian, J. C. S. Davis, E. Fradkin, and S. A. Kivelson, *Pair density waves in superconducting vortex halos*, *Phys. Rev. B* **97**, 174510 (2018), [arXiv:1802.01582](#) [[cond-mat.supr-con](#)].
- [22] M. Grandadam, D. Chakraborty, and C. Pépin, *Fractionalizing a Local Pair Density Wave: a Good “Recipe” for Opening a Pseudogap*, *Journal of Superconductivity and Novel Magnetism* **33**, 2361 (2020), [arXiv:1909.06657](#) [[cond-mat.supr-con](#)].
- [23] Y.-H. Liu, W.-L. Tu, G.-W. Chern, and T.-K. Lee, *Intertwined orders and electronic structure in superconducting vortex halos*, *Physical Review Research* **5**, 033028 (2023), [arXiv:2212.05685](#) [[cond-mat.supr-con](#)].
- [24] S. A. Kivelson, I. P. Bindloss, E. Fradkin, V. Oganesyan, J. M. Tranquada, A. Kapitulnik, and C. Howald, *How to detect fluctuating stripes in the high-temperature superconductors*, *Rev. Mod. Phys.* **75**, 1201 (2003).
- [25] P. A. Lee, *Amperean Pairing and the Pseudogap Phase of Cuprate Superconductors*, *Physical Review X* **4**, 031017 (2014), [arXiv:1401.0519](#) [[cond-mat.str-el](#)].
- [26] Z. Dai, T. Senthil, and P. A. Lee, *Modeling the pseudogap metallic state in cuprates: Quantum disordered pair density wave*, *Phys. Rev. B* **101**, 064502 (2020), [arXiv:1906.01656](#) [[cond-mat.str-el](#)].
- [27] M. Christos, Z.-X. Luo, H. Shackleton, Y.-H. Zhang, M. S. Scheurer, and S. Sachdev, *A model of d-wave superconductivity, antiferromagnetism, and charge order on the square lattice*, *Proceedings of the National Academy of Sciences* **120**, e2302701120 (2023), [arXiv:2302.07885](#) [[cond-mat.str-el](#)].
- [28] Y.-H. Zhang and S. Sachdev, *From the pseudogap metal to the Fermi liquid using ancilla qubits*, *Physical Review Research* **2**, 023172 (2020), [arXiv:2001.09159](#) [[cond-mat.str-el](#)].
- [29] S. Chatterjee and S. Sachdev, *Fractionalized Fermi liquid with bosonic chargons as a candidate for the pseudogap metal*, *Phys. Rev. B* **94**, 205117 (2016), [arXiv:1607.05727](#) [[cond-mat.str-el](#)].
- [30] E. Mascot, A. Nikolaenko, M. Tikhonovskaya, Y.-H. Zhang, D. K. Morr, and S. Sachdev, *Electronic spectra with paramagnon fractionalization in the single-band Hubbard model*, *Phys. Rev. B* **105**, 075146 (2022), [arXiv:2111.13703](#) [[cond-mat.str-el](#)].
- [31] M. Christos and S. Sachdev, *Emergence of nodal Bogoliubov quasiparticles across the transition from the pseudogap metal to the d-wave superconductor*, *npj Quantum Materials* **9**, 4 (2024), [arXiv:2308.03835](#) [[cond-mat.str-el](#)].
- [32] P. M. Bonetti, M. Christos, and S. Sachdev, *Quantum oscillations in the hole-doped cuprates and the confinement of spinons*, (2024), [arXiv:2405.08817](#) [[cond-mat.str-el](#)].
- [33] M. Christos, H. Shackleton, S. Sachdev, and Z.-X. Luo, *Deconfined quantum criticality of nodal d-wave superconductivity, Néel order, and charge order on the square lattice at half-filling*, (2024), [arXiv:2402.09502](#) [[cond-mat.str-el](#)].
- [34] P. A. Lee, N. Nagaosa, and X.-G. Wen, *Doping a Mott insulator: Physics of high-temperature superconductivity*, *Rev. Mod. Phys.* **78**, 17 (2006), [cond-mat/0410445](#).
- [35] S. Sachdev, *Stable hc/e vortices in a gauge theory of superconductivity in strongly correlated systems*, *Phys. Rev. B* **45**, 389 (1992).
- [36] N. Nagaosa and P. A. Lee, *Ginzburg-Landau theory of the spin-charge-separated system*, *Phys. Rev. B* **45**, 966 (1992).
- [37] P. A. Lee and X.-G. Wen, *Vortex structure in underdoped cuprates*, *Phys. Rev. B* **63**, 224517 (2001), [arXiv:cond-mat/0008419](#) [[cond-mat.str-el](#)].
- [38] L. Balents, L. Bartosch, A. Burkov, S. Sachdev, and K. Sengupta, *Putting competing orders in their place near the Mott transition. II. The doped quantum dimer model*, *Phys. Rev. B* **71**, 144509 (2005), [arXiv:cond-mat/0409470](#) [[cond-mat.str-el](#)].
- [39] L. Bartosch, L. Balents, and S. Sachdev, *Detecting the quantum zero-point motion of vortices in the cuprate*

- superconductors*, *Annals of Physics* **321**, 1528 (2006), [arXiv:cond-mat/0602429](#) [cond-mat.supr-con].
- [40] L. Balents and S. Sachdev, *Dual vortex theory of doped Mott insulators*, *Annals of Physics* **322**, 2635 (2007), [arXiv:cond-mat/0612220](#) [cond-mat.str-el].
- [41] J. Alicea, *Monopole quantum numbers in the staggered flux spin liquid*, *Phys. Rev. B* **78**, 035126 (2008), [arXiv:0804.0786](#) [cond-mat.str-el].
- [42] X.-Y. Song, Y.-C. He, A. Vishwanath, and C. Wang, *From spinon band topology to the symmetry quantum numbers of monopoles in Dirac spin liquids*, *Phys. Rev. X* **10**, 011033 (2020), [arXiv:1811.11182](#) [cond-mat.str-el].
- [43] Y.-H. Zhang and S. Sachdev, *Deconfined criticality and ghost Fermi surfaces at the onset of antiferromagnetism in a metal*, *Phys. Rev. B* **102**, 155124 (2020), [arXiv:2006.01140](#) [cond-mat.str-el].
- [44] P. A. Lee and X.-G. Wen, *Vortex structure in underdoped cuprates*, *Physical Review B* **63**, 224517 (2001), [cond-mat/0008419](#).
- [45] V. N. Muthukumar and Z. Y. Weng, *Ginzburg-landau theory of a resonating-valence-bond superconductor*, *Phys. Rev. B* **65**, 174511 (2002).
- [46] Z.-J. Song, J.-X. Zhang, and Z.-Y. Weng, *Thermal Hall Effect and Neutral Spinons in a Doped Mott Insulator* (2023), [arXiv:2309.05711](#).
- [47] M. Franz and Z. Tešanović, *Vortex state in a doped Mott insulator*, *Physical Review B* **63**, 064516 (2001), [cond-mat/0002137](#).
- [48] V. Juričić, I. F. Herbut, and Z. Tešanović, *Restoration of the Magnetic hc/e -Periodicity in Unconventional Superconductors*, *Physical Review Letters* **100**, 187006 (2008), 0711.3790.
- [49] M. Franz and Z. Tešanović, *Quasiparticles in the Vortex Lattice of Unconventional Superconductors: Bloch Waves or Landau Levels?*, *Physical Review Letters* **84**, 554 (1999), [cond-mat/9903152](#).
- [50] O. Vafek, A. Melikyan, M. Franz, and Z. Tešanović, *Quasiparticles and vortices in unconventional superconductors*, *Physical Review B* **63**, 134509 (2001), [cond-mat/0007296](#).
- [51] O. Vafek, A. Melikyan, and Z. Tešanović, *Quasiparticle Hall transport of d-wave superconductors in the vortex state*, *Physical Review B* **64**, 224508 (2001), [cond-mat/0104516](#).
- [52] P. Nikolić, S. Sachdev, and L. Bartosch, *Electronic states near a quantum fluctuating point vortex in a d-wave superconductor: Dirac fermion theory*, *Physical Review B* **74**, 144516 (2006), [cond-mat/0606001](#).
- [53] P. Nikolić and S. Sachdev, *Effective action for vortex dynamics in clean d-wave superconductors*, *Physical Review B* **73**, 134511 (2006), [cond-mat/0511298](#).
- [54] A. Melikyan and Z. Tešanović, *Dirac-Bogoliubov-deGennes quasiparticles in a vortex lattice*, *Physical Review B* **76**, 094509 (2007), [cond-mat/0605314](#).